



HAL
open science

Identification of the *Arabidopsis* calmodulin-dependent NAD⁺ kinase that sustains the elicitor-induced oxidative burst

Elisa Dell'Aglio, Cécile Giustini, Alexandra Kraut, Yohann Couté, Alex Costa, Guillaume Decros, Yves Gibon, Christian Mazars, Michel Matringe, Giovanni Finazzi, et al.

► To cite this version:

Elisa Dell'Aglio, Cécile Giustini, Alexandra Kraut, Yohann Couté, Alex Costa, et al.. Identification of the *Arabidopsis* calmodulin-dependent NAD⁺ kinase that sustains the elicitor-induced oxidative burst. *Plant Physiology*, 2019, 181 (4), pp.1449-1458. 10.1104/pp.19.00912 . hal-02361156

HAL Id: hal-02361156

<https://hal.science/hal-02361156>

Submitted on 13 Nov 2019

HAL is a multi-disciplinary open access archive for the deposit and dissemination of scientific research documents, whether they are published or not. The documents may come from teaching and research institutions in France or abroad, or from public or private research centers.

L'archive ouverte pluridisciplinaire **HAL**, est destinée au dépôt et à la diffusion de documents scientifiques de niveau recherche, publiés ou non, émanant des établissements d'enseignement et de recherche français ou étrangers, des laboratoires publics ou privés.

1 **The Arabidopsis Calmodulin-dependent NAD⁺ kinase sustaining the elicitor-induced oxidative**
2 **burst**

3 Elisa Dell'Aglio^{a,b}, Cécile Giustini^a, Alexandra Kraut^c, Yohann Couté^c, Alex Costa^d, Guillaume Decros^e,
4 Yves Gibon^{e,f}, Christian Mazars^g, Michel Matringe^a, Giovanni Finazzi^a, Gilles Curien^{a*}

5 ^a Univ. Grenoble Alpes, CNRS, CEA, INRA, BIG-LPCV, 38000 Grenoble, France

6 ^b Department of Botany and Plant Biology, University of Geneva, 1211 Geneva, Switzerland

7 ^c Univ. Grenoble Alpes, CEA, INSERM, BIG-EdyP, 38000 Grenoble, France

8 ^d Department of Biosciences, University of Milan, 20133 Milan, Italy

9 ^e UMR1332 BFP, INRA, Univ. Bordeaux, Villenave d'Ornon, France

10 ^f MetaboHUB, Bordeaux, Villenave d'Ornon, France

11 ^g Laboratoire de Recherche en Sciences Végétales, Université de Toulouse, CNRS, UPS, 24, Chemin
12 de Borde-Rouge, Auzeville, BP 42617, 31326 Castanet-Tolosan, France.

13 * To whom correspondence may be addressed. E-mail: gilles.curien@cea.fr

14

15 Running title: Plant calmodulin-dependent NAD⁺ kinase

16

17 **Abstract**

18 NADP(H) is an essential cofactor of multiple metabolic processes in all living organisms. In plants,
19 NADP(H) is required as the substrate of Ca²⁺-dependent NADPH oxidases which catalyze a reactive
20 oxygen species burst in response to various stimuli. While NADP⁺ production in plants has long been
21 known to involve a Calmodulin and Calcium (CaM)/Ca²⁺- dependent NAD⁺ kinase, the nature of the
22 enzyme catalyzing this activity has remained enigmatic, as well as its role in plant physiology. Here,
23 thanks to a combination of proteomics, biochemistry, molecular biology and *in vivo* studies, we have
24 identified an Arabidopsis protein that catalyzes NADP⁺ production exclusively in the presence of
25 CaM/Ca²⁺. This new enzyme (NADKc) has a CaM-binding peptide located in its N-terminal region and
26 displays peculiar biochemical properties as well as different domain organization compared to known
27 plant NAD⁺ kinases. In response to a pathogen elicitor, activity of NADKc, which is associated with the
28 mitochondrial periphery, contributes to an increase in the cellular NADP⁺ concentration and to the
29 amplification of the elicitor-induced oxidative burst. Based on a phylogenetic analysis and enzymatic
30 assays, we propose that the CaM/Ca²⁺-dependent NAD⁺ kinase activity found in photosynthetic

- 1 organisms is carried out by NADKc-related proteins. Thus, NADKc represents the missing link between
- 2 Ca^{2+} signalling, metabolism and the oxidative burst.
- 3 **Keywords:** NAD^+ kinase, Calmodulin, Calcium, NADP^+ , zeta toxin, flagellin22, *Arabidopsis thaliana*.

1 **Introduction**

2 As sessile organisms, plants have evolved mechanisms to react quickly to stress conditions, such as
3 changes in temperature, salinity or pathogen attacks. A common response to stress is a cytosolic calcium
4 (Ca^{2+}) influx followed by an apoplastic burst of Reactive Oxygen Species, or ROS burst (Grant et al.,
5 2000). This ROS burst is generated by plasma membrane NADPH oxidases known as RBOH (for
6 Respiratory Burst Oxidase Homologs, Torres and Dangl, 2005) and in turn regulates adaptation
7 mechanisms such as gene expression, epigenetic changes and long-distance signal transduction
8 (Liebthal and Dietz, 2017; Choi et al., 2017; Chapman et al., 2019). RBOH oxidase activity is dependent
9 on Ca^{2+} binding to their EF-hand domains and is stimulated by phosphorylation by Ca^{2+} -dependent
10 Protein Kinases (Dubiella et al., 2013) as well as CIPK/CBL complexes (Calcineurin B-Like Protein -
11 CBL-Interacting Protein Kinase, Drerup *et al.*, 2013).

12 A rapid increase in the NADP(H) pool size was observed in response to plant treatment with a pathogen
13 elicitor (Harding et al., 1997; Pugin et al., 1997) and may be required to sustain the ROS burst by fuelling
14 RBOH proteins. Since most (~70-90%) of plant NAD^+ kinase activity is dependent on binding
15 Calmodulin (CaM) in its Ca^{2+} -loaded conformation (Anderson and Cormier, 1978) it was proposed
16 (Harding et al., 1997) that the protein responsible for this activity may also be stimulated by the elicitor-
17 induced Ca^{2+} influx. NADP^+ produced by this enzyme may then be converted to NADPH (the substrate
18 of RBOH proteins) by NADP-isocitrate dehydrogenase (Mhamdi et al., 2010) or by the reducing branch
19 of the oxidative pentose phosphate pathway (Pugin et al., 1997; Scharte et al., 2009).

20 Several studies have described the CaM/ Ca^{2+} -dependent NAD^+ kinase activity in plants using partially
21 purified enzymatic preparations from plant tissues. These studies allowed to find this protein activity in
22 a wide variety of plant species (Dieter and Marmé, 1984; Delumeau et al., 2000; Turner et al, 2004),
23 and to characterize its kinetic parameters (Delumeau et al., 2000; Turner et al., 2004) as well as its
24 preferences for specific CaM and CaM-like isoforms (Turner et al., 2004). However, the protein
25 responsible for CaM/ Ca^{2+} -dependent NAD^+ kinase activity has not been identified. In particular, among
26 the three Arabidopsis NAD^+ kinases identified to date, the plastidial NADK2 was shown to bind CaM
27 *in vitro* in a Ca^{2+} -dependent way (Dell'Aglio et al., 2013a; Turner et al., 2004), but its activity does not

1 require CaM binding (Turner et al., 2004). Thus, this lack of knowledge of the identity of the plant CaM-
2 dependent NAD⁺ kinase has prevented a thorough characterization of its role in plant physiology, and
3 in particular in the production of the stress-induced ROS burst.

4 Here, we report the characterization of an *A. thaliana* CaM/Ca²⁺-dependent NAD⁺ kinase that displays
5 all the properties of the elusive enzyme. We show that this NAD⁺ kinase, which we named NADKc (for
6 NAD kinase-CaM dependent), is associated with mitochondrial periphery and is involved in sustaining
7 the ROS burst induced by the bacterial elicitor flagellin22.

8 **Results and discussion**

9 **NADKc is a new CaM/Ca²⁺-dependent NAD⁺ kinase**

10 We obtained an Arabidopsis protein extract enriched in CaM/Ca²⁺-dependent NAD⁺ kinase activity by
11 a four-step purification procedure described in Supplemental Material and Methods. The last step
12 consisted in binding the protein on a CaM-charged matrix in the presence of Ca²⁺ and its subsequent
13 release with an excess of the Ca²⁺ chelator EGTA (Fig. S1). We then used mass spectrometry-based
14 proteomics to identify proteins that were enriched in the EGTA elution compared to the Ca²⁺-containing
15 washing steps (Supplemental Table S1). We reasoned that putative CaM/Ca²⁺-dependent NAD⁺ kinases
16 should display the following characteristics: *i*) have a molecular weight between 50 and 65 kDa, to
17 respect the size range previously calculated by Delumeau et al., 2000; *ii*) be annotated as ATP-binding
18 proteins (but not as a protein kinase), since it is known that plant CaM-activated NAD kinase uses ATP
19 as a substrate (Anderson and Cormier, 1978); *iii*) contain a predicted CaM-binding site (following the
20 guidelines of Rhoads and Friedberg, 1997) and *iv*) have no previously assigned enzymatic activity. Our
21 analysis revealed only one protein – encoded by the At1g04280 gene – that fulfilled all these criteria.

22 To confirm its CaM/Ca²⁺-dependent NAD⁺ kinase activity, we expressed the full-length recombinant
23 protein coded by At1g04280 in *E. coli* with an N-terminal His-tag. We compared the NAD⁺ kinase
24 activity of two *E. coli* extracts: one obtained from an At1g04280-expressing strain and the second from
25 a strain containing an empty vector. As shown in Fig. 1A, no NAD⁺ kinase activity (which in our test
26 was detected as an increase of absorbance at 340 nm) was detected in the *E. coli* strain containing the

1 empty vector, not even after the addition of an excess of Ca^{2+} and of *A. thaliana* Calmodulin 1 (AtCaM1).
2 In contrast, addition of the At1g04280-expressing *E. coli* extract to the same reaction mixture
3 immediately revealed NAD^+ kinase activity.

4 Activity measurements with a partially purified At1g04280 enzyme confirmed the lack of NAD^+ kinase
5 activity in the absence of AtCaM1/ Ca^{2+} and its appearance, within seconds, upon addition of both
6 AtCaM1 and Ca^{2+} . This NAD^+ kinase activity was suppressed by EGTA and restored by the addition of
7 an excess of Ca^{2+} , showing that the CaM/ Ca^{2+} -dependent enzyme activation is an all-or-none, reversible
8 process (Fig. 1B). In contrast, while a CaM/ Ca^{2+} -dependent NAD^+ kinases have also been described in
9 invertebrates, animal NAD^+ kinase activity is only slightly increased by CaM/ Ca^{2+} addition. For
10 example, CaM induces a 3.5-fold increase of the NADK-2 activity of the sea urchin *Strongylocentrotus*
11 *purpuratus* (Love et al., 2015).

12 Based on these results, we identified the At1g04280 gene product as the long-sought CaM/ Ca^{2+} -
13 dependent NAD^+ kinase enzyme previously found in several plant species (Anderson and Cormier,
14 1978, Delumeau et al., 1998, Turner et al., 2004) and named it *A. thaliana* “NADKc” for “NAD kinase-
15 CaM dependent”.

16 **AtNADKc peculiar features in primary sequence and enzyme activity**

17 The primary sequence of NADKc (Fig. 1C) contains: *i*) an N-terminal region predicted to contain a
18 transmembrane helix (amino acids: 1-45); *ii*) a domain of unknown function (amino acids 46-225) that
19 includes a conserved putative CaM-Binding Site (CBS, Fig S2A); and *iii*) a C-terminal kinase domain
20 (amino acids 226-340) similar to bacterial type II zeta-toxin domains (Khoo et al., 2007), which is
21 predicted to contain a conserved P-loop for ATP binding (Walker A motif, WM, amino acids: 236-250,
22 Fig S2B). Interestingly, these features are not shared with all other NAD^+ kinases known to date, from
23 bacteria, plants and animals (Fig. 1C, Kawai et al, 2001; Turner et al., 2004, Chai et al., 2006; Love et
24 al., 2015).

25 To optimize NADKc expression levels in *E. coli* and improve the solubility of the protein, we removed
26 the first 38 residues constituting the predicted transmembrane helix. The shorter version, 6HIS-

1 $\Delta 38\text{NADKc}$ was partially purified by Ni-NTA affinity chromatography (Fig. S3, lane 3). Activity assays
2 with saturating AtCaM1/ Ca^{2+} concentrations revealed the NAD^+ kinase activity of NADKc to be
3 specific toward NAD^+ , as no activity could be detected with NADH or deamido- NAD^+ (NAAD) (Table
4 1). Like most P-loop-containing kinases (Das et al., 2013), the enzyme displayed broad specificity for
5 the phosphoryl donor, as ATP, CTP, GTP and UTP could be used indifferently and produced similar
6 efficiencies (Table 1). The enzyme catalytic constant with CTP or ATP was close to 40 s^{-1} in the presence
7 of Ca^{2+} and AtCaM1, *i.e.* about 10-fold higher than that reported for plant CaM/ Ca^{2+} -independent NAD^+
8 kinases and other NAD^+ kinases from bacteria and animals ($0.5\text{-}7 \text{ s}^{-1}$, (Kawai et al., 2001; Chai et al.,
9 2006; Love et al., 2015; Turner et al., 2004)).

10 To characterize the interaction of NADKc with CaM, we further purified the recombinant enzyme by
11 urea denaturation and rapid dilution (see Supplemental Material & Methods). The refolded protein (Fig
12 S3, lanes 4-5) produced a single band on an SDS-PAGE gel and had an increased catalytic constant (70
13 s^{-1}) compared to the partially purified enzyme (40 s^{-1} , Table 1) and high affinity for CaM ($k_d = 0.6\text{-}1 \text{ nM}$,
14 Fig. 1D), similar to the value of 0.4 nM reported for the tomato CaM-dependent NAD^+ kinase
15 (Delumeau et al., 2000).

16 In conclusion, compared to all other NAD^+ kinases known to date, NADKc displays unique structural
17 as well as catalytic features which make it particularly suitable for rapid NADP^+ production following
18 Ca^{2+} signals.

19 **Identification of a CaM-binding peptide in the NADKc N-terminal domain**

20 To verify that the NADKc N-terminal domain is involved in CaM-binding, we measured NADKc
21 activity in the presence of a synthetic peptide containing the putative “type A 1-8-14” CaM-binding
22 sequence (amino acids 167-196, Fig. 1C, Rhoads and Friedberg, 1997) in a competitive assay. As shown
23 in Fig. 1E, the presence of the putative NADKc CaM-binding peptide decreased the stimulation of
24 NADKc by AtCaM1, as expected if AtCaM1, trapped by the peptide in excess, was no longer available
25 for NADKc activation. The reduction in reaction rate was hyperbolically related to the peptide
26 concentration ($\text{IC}_{50} = 0.5 \text{ }\mu\text{M}$). In contrast, another unrelated peptide from the Tic32 protein, which

1 cannot specifically bind AtCaM1 (Dell'Aglio, 2013b), was also tested. An excess of this control peptide
2 had no effect on NAD⁺ kinase activity (Fig. 1E).

3 These data suggest that the NADKc peptide identified plays a major role in the AtCaM1/Ca²⁺-dependent
4 activation of the NADKc enzyme. We hypothesize that it could be an anchoring point for CaM in the
5 full-length protein, facilitating activation of the kinase domain by an as yet unknown mechanism.

6 **NADKc is located at the mitochondrial periphery**

7 To assess the NADKc localization *in vivo*, we produced strains containing several YFP-tagged NADKc
8 versions: *i.*) the NADKc full-length protein fused to YFP at its C-terminal (construct NADKc-YFP); *ii.*)
9 the NADKc N-terminal region (amino acids 1-45) fused to YFP (construct NADK_{C_{Nter}}-YFP); the YFP
10 fused at the N-terminus of the whole NADKc protein sequence (construct YFP-NADKc). All fusion
11 proteins were inserted into expression plasmids under the control of the CaMV 35S promoter.

12 Arabidopsis lines and tobacco leaves containing the NADKc:YFP construct showed protein clusters that
13 likely constitute non-specific aggregates caused by high expression of a membrane construct (not
14 shown). However, in tobacco leaves (see Fig. S4, upper and middle row) and Arabidopsis seedlings, the
15 NADK_{C_{Nter}}-YFP was targeted to ring-like structures in both stomata (Fig. 2 A-F) and root tip cells. In
16 the root tips, the NADK_{C_{Nter}}-YFP protein co-localized with the mitochondrial matrix marker
17 Tetramethylrhodamine, methyl ester (TMRM), but the fluorescence signal of NADK_{C_{Nter}}-YFP was more
18 peripheral than the TMRM signal (Fig. 2, G-I). As a comparison, we observed Arabidopsis root tip cells
19 expressing NMT1-GFP, an outer mitochondrial membrane protein (Fig. 2, J-L, Wagner et al., 2015), as
20 well as MT-cp-YFP (Fig. 2, M-O), a pH biosensor located in the mitochondrial matrix (Schwarzländer
21 et al., 2011; Behera et al., 2018). This comparison clearly showed a higher resemblance of the
22 NADK_{C_{Nter}}-YFP signal profile to the NMT1-GFP profile than to the MTcp-YFP profile, suggesting a
23 localization at the outer mitochondrial membrane.

24 To corroborate this conclusion we measured the pixel intensity distribution of various TMRM-stained
25 mitochondria from NADK_{C_{Nter}}-YFP transformed plants. While the TMRM fluorescence intensity peak
26 was located at the centre of the mitochondria, NADK_{C_{Nter}}-YFP fluorescence intensity formed two

1 distinctive peaks at opposite sides from the centre where fluorescence intensity was at its minimum (Fig.
2 2, P-R). This pattern matches the one previously measured for the outer-membrane localized NMT1-
3 GFP protein (Wagner et al, 2015).

4 We successfully achieved expression of YFP-NADKc only in transiently transformed tobacco leaves,
5 where fluorescence was dispersed inside the cytosol (Fig. S4, bottom line). This result was probably due
6 to the NADKc N-terminus being hidden in the middle of the sequence and is consistent with the
7 hypothesis that the N-terminal region of NADKc is important for the protein to be correctly addressed
8 to the mitochondria.

9 Protein overexpression by a strong promoter as CaMV 35S is prone to promote protein aggregates and
10 overexpression artefacts. However, using cell fractionation, early works on the CaM/Ca²⁺-dependent
11 NAD⁺ kinase activity in plants located this enzyme at the mitochondrial periphery (either inner or outer
12 mitochondrial membrane) in both maize (Dieter and Marmé, 1984; Sauer and Robinson, 1985) and
13 *Avena sativa* (Pou de Crescenzo et al., 2001). More recently, NADKc was detected in the mitochondria
14 by two proteomic studies (Klodmann et al., 2011, Wagner et al., 2015) and at the plasma membrane by
15 one study (Mitra et al., 2009). Our results therefore corroborate and extend previous findings obtained
16 using different approaches.

17 **NADKc enhances Flg22 response in Arabidopsis seedlings**

18 To investigate the physiological role of NADKc, we analysed the two Arabidopsis T-DNA insertion
19 lines SALK_006202 and GABI-KAT 311H11, hereafter called *nadkc-1* and *nadkc-2* (Fig. 3A). NADKc
20 transcripts were reduced by more than 95% in both lines (Fig. 3B).

21 To confirm the unique role of NADKc for CaM/Ca²⁺-dependent NADP⁺ production in Arabidopsis
22 seedlings, NAD⁺ kinase activity was measured in protein extracts from Col-0 and mutant seedlings, both
23 in the presence of trifluoroperazine (TFP) - a CaM inhibitor - and AtCaM1/Ca²⁺ (Fig. 3C). In Col-0
24 plants, the activity measured in the presence of AtCaM1/Ca²⁺ was more than 10-fold higher than in the
25 presence of TFP, while in *nadkc-1/2* mutants, no difference was observed between the two conditions.
26 In both mutants, activity levels were close to those measured in Col-0 plants in the presence of TFP,

1 confirming the absence of NADKc activity in these mutants. Consistent with these results, two
2 complemented lines obtained by stably transforming *nadkc-1* with full-length NADKc under the control
3 of the CaMV 35S promoter (lines *nadkc-1_NADKc-1* and *nadkc-1_NADKc-2*) - had NADKc activity
4 levels similar to Col-0 (Fig. 4D).

5 Neither *nadkc* mutant showed any visible growth impairment when grown under short day or long day
6 photoperiods (Fig. S5, A-B) and photosynthetic parameters (Fv/Fm, ETR and NPQ, (Maxwell and
7 Johnson, 2000)) were the same in all genotypes (Fig. S5, C-E). This suggests that NADKc is not
8 involved in photosynthesis-driven growth.

9 As CaM-dependent NAD⁺ kinase activity was previously associated with the generation of the oxidative
10 burst triggered by plant response to elicitors (Grant et al., 2000; Harding et al., 1997), we expected to
11 observe a decrease in a pathogen elicitor-induced extracellular ROS burst in *nadkc-1/2* mutants coupled
12 with lower NADP pools with respect to Col-0 seedlings.

13 We therefore exposed 7-day-old Arabidopsis seedlings to the bacterial elicitor flg22, followed by
14 measurements of NAD(P)⁺ and NAD(P)H concentrations and ROS production. As shown in Fig. 3E, no
15 statistically significant differences were observed between Col-0 and *nadkc-1* in NAD(P)⁺ and
16 NAD(P)H concentrations before the flg22 treatment. However, the flg22 challenge induced an increase
17 in the Col-0 NADP⁺ cellular concentration, which was absent in the *nadkc* seedlings. Moreover,
18 dramatic reduction in ROS accumulation (more than 90%) was observed in the *nadkc-1/2* mutants (Fig.
19 3F), but complementation with the NADKc full-length protein restored ROS accumulation up to wild-
20 type levels (Fig. 3G).

21 Based on these results, we propose a role for NADKc in producing NADP(H) needed to sustain the
22 elicitor-induced ROS burst in Arabidopsis seedlings (Fig. 4).

23 **Distribution of CaM-dependent NAD⁺ kinase activity in the green lineage**

24 The domain organization of NADKc (*i.e.*, a ca 200 amino acid domain of unknown function at the N-
25 terminus with a putative CBS followed by a kinase domain annotated “zeta toxin domain”, Fig. 1C) was
26 only found in higher plants and some algae.

1 To better trace the evolution of the plant CaM-dependent NAD⁺ kinase, we compared gene sequences
2 and NADK activity in several plants and algae and we built a maximum likelihood phylogenetic tree
3 with representative putative NADKc proteins (Fig. S6). The phylogenetic tree showed that plant
4 NADKc-like proteins form four major clusters that correspond to the main plant phylogenetic groups
5 with the exception of Gymnosperms and Pteridophytes. Many plants, especially dicots, contain several
6 genes encoding for this protein, suggesting duplication events across evolution. Interestingly, the two
7 other NADKc homologues present in the Arabidopsis genome (At1g06750 and At2g30630) seem to
8 have a pollen-specific expression pattern (Krishnakumar et al., 2014).

9 Among algae, while the genomes of *Chlamydomonas reinhardtii*, *Ostreococcus taurii* and *Chara*
10 *braunii* appeared devoid of NADKc-like sequences, the genomes of *Coccomyxa subellipsoidea*, *Ulva*
11 *mutabilis*, *Klebsormidium flaccidum*, *Spyrotaenia minuta*, *Entransia fimbriata*, Mougeotia sp. and
12 Spirogyra sp. all harbour one NADKc-like sequence. In particular, NAD⁺ kinase genes of
13 *Klebsormidium flaccidum*, *Entransia fimbriata*, Mougeotia sp. and Spirogyra sp. contain a clear CBS,
14 while in *Coccomyxa subellipsoidea*, *Ulva mutabilis* and *Spirotaenia minuta*, this region is less conserved
15 (Fig. S2A). In agreement with the genomic survey, CaM-dependent NAD⁺ kinase activity could be
16 successfully measured in the moss *M. polymorpha* and filamentous alga *K. flaccidum*, but not in the
17 unicellular alga *C. reinhardtii* (Table 2).

18 Interestingly, both the total CaM-dependent NAD⁺ kinase activity and the percentage of CaM-dependent
19 NADK-activity on the total NADK activity increase from *K. flaccidum* (4.0 nmol·h⁻¹·mg⁻¹; 66.7%) to
20 *M. polymorpha* (5.9 nmol·h⁻¹·mg⁻¹; 85.7%) and to *A. thaliana* (30.2 nmol·h⁻¹·mg⁻¹; 96.8%). It is
21 therefore possible that the importance of the CaM control on NADKc-like proteins increased during the
22 evolution of plant lineage and became a key element of the ROS response to elicitors in angiosperms,
23 and quite likely other abiotic/biotic stress conditions that trigger Ca²⁺ fluxes.

24 **Conclusions**

25 Overall, we have identified unambiguously NADKc as the CaM/Ca²⁺-dependent NAD⁺ kinase of
26 Arabidopsis seedlings. Its identification allows answering earlier questions concerning its physiological

1 role: consistent with its localization at the mitochondrial periphery, this enzyme has no role in
2 photosynthesis, but can regulate the ROS burst by sustaining the activity of RBOH proteins. Besides
3 being essential for the elicitor-induced oxidative burst of Arabidopsis, this enzyme may participate in
4 other plant developmental and stress responses involving Ca^{2+} fluxes. This would stem from the
5 evolutionary recruitment of a distinctive combination of a CaM-binding region and a type II zeta-toxin
6 domain, which would provide it with regulatory properties different from its animal counterpart.

7

8 **Material and Methods**

9 **Chemicals**

10 All chemicals were from Sigma Aldrich.

11 **Plant growth and isolation of homozygous NADKc lines**

12 *A. thaliana* Col-0 ecotype was used in this study. Plants were grown under 65% humidity and either
13 long day (16 h light – 85 $\mu\text{mol photons}\cdot\text{m}^{-2}\cdot\text{s}^{-1}$, 8 h dark) or short day (8 h light – 90 $\mu\text{mol photons}\cdot\text{m}^{-2}\cdot\text{s}^{-1}$, 16 h dark) conditions. Day-time temperature was set to 20 °C, and night-time temperature to 18
14 °C.
15 °C.

16 The two T-DNA insertion lines, *nadkc-1* (SALK_006202) and *nadkc-2* (GABI_311H11), were obtained
17 from NASC/ABRC (Alonso et al., 2003; Kleinboelting et al., 2012). Lines were selected in the
18 appropriate antibiotic (kanamycin for *nadkc-1* and sulfadiazine for *nadkc-2*) and genotyped by PCR
19 using left border primers LBb1.3 (*nadkc-1*) or LB GABI-KAT (*nadkc-2*) and the appropriate specific
20 primers listed in Supplemental Table S2. PCR products were sequenced to confirm the precise position
21 of each insertion.

22 *Klebsormidium flaccidum* (Hori et al., 2014) (SAG335-2b curated as *Klebsormidium nitens*) was
23 obtained from EPSAG (Department of Experimental Phycology and Culture Collection of Algae,
24 Göttingen Universität, Germany). The alga was grown on agar plates under continuous light (60 μmol

1 photons·m⁻²·s⁻¹) in the Modified Bolds 3N Medium (<https://utex.org/products/modified-bolds-3n>
2 medium) without vitamins.

3 *M. polymorpha* was collected in the forest (GPS coordinate: 45.335088 , 5.632257) and *Chlamydomonas*
4 *reinhardtii* (C137 strain) was grown in TAP medium at 24°C under continuous low white light (40 μmol
5 photons·m⁻²·s⁻¹) exposure. Protein extracts were prepared as described in the supplementary information
6 for Arabidopsis.

7 Additional Material and Methods procedures are described in the Supplementary Information.

8 **Author contributions**

9 E.D., C.M., G.F. and G.C. designed the experiments and analyzed the data; E.D., C.G., M.M., A.K.,
10 Y.C., A.C. G.F., C.M., G.D., Y.G. and G.C. conducted the experiments. E.D., G.F., C.M. and G.C. wrote
11 the article with contributions from all the authors. G.C. agrees to serve as the author responsible for
12 contact and ensures communication.

13 **Accession numbers**

14 Sequence data from this article can be found in the EMBL/GenBank data libraries under accession
15 number: At1g04280; UniProt accession: Q0WUY1.

16

17 **Acknowledgments**

18 This work was supported by the French National Research Agency (grant no. ANR-10-13 LABEX-04
19 GRAL Labex, Grenoble Alliance for Integrated Structural Cell Biology). G.F. acknowledges support
20 from the HFSP grant RGP0052/2015 (photosynthetic light utilization and ion fluxes: making the link)
21 and A.C. to UNIMI PIANO DI SVILUPPO DI ATENEO, Transition Grant 2015/2017 – Horizon 2020
22 Linea 1A. The proteomic analyses were partially supported by the French National Research Agency
23 ProFI Grant (ANR-16 10-INBS-08-01). Part of this work was carried out at NOLIMITS, an advanced
24 imaging facility established by the University of Milan.

1 We are grateful to Markus Schwarzländer (University of Münster, Germany) for providing the
2 NMT1:GFP and MT-cp:YFP Arabidopsis lines. We thank Elsa Clavel-Coibrié for help with analysis of
3 the complemented mutant plants.

4 **References**

- 5 **Alonso JM, Stepanova AN, Leisse TJ, Kim CJ, Chen H, Shinn P, Stevenson DK,**
6 **Zimmerman J, Barajas P, Cheuk R, et al** (2003) Genome-wide insertional mutagenesis of
7 *Arabidopsis thaliana*. *Science* **301**: 653-657
- 8 **Anderson JM, Cormier MJ** (1978) Calcium-dependent regulation of NAD kinase. *Biochem*
9 *Biophys Res Commun* **84**: 595-602
- 10 **Behera S, Zhaolong X, Luoni L, Bonza MC, Doccua FG, De Michelis MI, Morris RJ,**
11 **Schwarzländer M, Costa A** (2018) Cellular Ca²⁺ signals generate defined pH signatures in plants. *Plant*
12 *Cell* **30**: 2704-2719
- 13 **Chai MF, Wei PC, Chen QJ, An R, Chen J, Yang S, Wang XC** (2006) NADK3, a novel
14 cytoplasmic source of NADPH, is required under conditions of oxidative stress and modulates abscisic
15 acid responses in Arabidopsis. *Plant J* **47**: 665-674
- 16 **Chapman JM, Muhlemann JK, Gayomba SR, Muday GK** (2019) RBOH-Dependent ROS
17 Synthesis and ROS scavenging by plant specialized metabolites to modulate plant development and
18 stress responses. *Chem Res Toxicol.* **32**: 370-396
- 19 **Choi WG, Miller G, Wallace I, Harper J, Mittler R, Gilroy S** (2017) Orchestrating rapid long-
20 distance signaling in plants with Ca²⁺, ROS and electrical signals. *Plant J* **90**: 698-707
- 21 **Dell'Aglio E, Giustini C, Salvi D, Brugiere S, Delpierre F, Moyet L, Baudet M, Seigneurin-**
22 **Berny D, Matringe M, Ferro M, et al** (2013a) Complementary biochemical approaches applied to the
23 identification of plastidial calmodulin-binding proteins. *Mol Biosyst* **9**: 1234-1248
- 24 **Dell'Aglio E** (2013b) The regulation of plastidial proteins by calmodulins: Université de
25 Grenoble.
- 26 **Delumeau O, Renard M, Montrichard F** (2000b) Characterization and possible redox
27 regulation of the purified calmodulin-dependent NAD⁺ kinase from *Lycopersicon pimpinellifolium*.
28 *Plant Cell Environ* **23**: 1267-1273
- 29 **Dieter P, Marme D** (1984) A Ca²⁺, Calmodulin-dependent NAD kinase from corn is located in
30 the outer mitochondrial membrane. *J Biol Chem* **259**: 184-189
- 31 **Drerup MM, Schlücking K, Hashimoto K, Manishankar P, Steinhorst L, Kuchitsu K, Kudla**
32 **J.** (2013) The Calcineurin B-like calcium sensors CBL1 and CBL9 together with their interacting protein
33 kinase CIPK26 regulate the Arabidopsis NADPH oxidase RBOHF. *Mol Plant.* **6**: 559-69
- 34 **Dubiella U, Seybold H, Durian G, Komander E, Lassig R, Witte CP, Schulze WX, Romeis**
35 **T** (2013) Calcium-dependent protein kinase/NADPH oxidase activation circuit is required for rapid
36 defense signal propagation. *Proc Natl Acad Sci USA.* **110**: 8744-9
- 37 **Grant M, Brown I, Adams S, Knight M, Ainsli A, Mansfield J** (2000) The RPM1 plant disease
38 resistance gene facilitates a rapid and sustained increase in cytosolic calcium that is necessary for the
39 oxidative burst and hypersensitive cell death. *Plant J* **23**: 441-450

- 1 **Harding SA, Oh SH, Roberts DM** (1997) Transgenic tobacco expressing a foreign calmodulin
2 gene shows an enhanced production of active oxygen species. *Embo J* **16**: 1137-1144
- 3 **Kawai S, Mori S, Mukai T, Hashimoto W, Murata K** (2001) Molecular characterization of
4 *Escherichia coli* NAD kinase. *Eur J Biochem* **268**: 4359-65
- 5 **Khoo SK, Loll B, Chan WT, Shoeman RL, Ngoo L, Yeo CC, Meinhart A** (2007) Molecular
6 and structural characterization of the PezAT chromosomal toxin-antitoxin system of the human
7 pathogen *Streptococcus pneumoniae*. *J Biol Chem* **282**: 19606-19618
- 8 **Kleinboelting N, Huet G, Kloetgen A, Viehoveer P, Weisshaar B** (2012) GABI-Kat
9 SimpleSearch: new features of the *Arabidopsis thaliana* T-DNA mutant database. *Nucleic Acids Res*
10 **40**: D1211-1215
- 11 **Klodmann J, Senkler M, Rode C, Braun H-P** (2011) Defining the protein complex proteome
12 of plant mitochondria. *Plant Phys* **157**: 587–598
- 13 **Krishnakumar V, Hanlon MR, Contrino S, Ferlanti ES, Karamycheva S, Kim M, Rosen**
14 **BD, Cheng C-Y, Moreira W, Mock SA, Stubbs J, Sullivan JM, Krampis K, Miller JR, Micklem**
15 **G, Vaughn M, Town CD** (2015) Araport: the Arabidopsis information portal. *Nucleic Acids Research*
16 **43**: D1003–D1009
- 17 **Love NR, Pollak N, Dolle C, Niere M, Chen Y, Oliveri P, Amaya E, Patel S, Ziegler M** (2015)
18 NAD kinase controls animal NADP biosynthesis and is modulated via evolutionarily divergent
19 calmodulin-dependent mechanisms. *Proc Natl Acad Sci USA* **112**: 1386-1391
- 20 **Liebthal M, Dietz KJ** (2017) The fundamental role of reactive oxygen species in plant stress
21 response. *Plant Stress Tolerance In: Sunkar R. (eds) Plant Stress Tolerance. Methods in Molecular*
22 *Biology*, **1631**: 23-39. Humana Press, New York, NY.
- 23 **Maxwell K, Johnson GN** (2000) Chlorophyll fluorescence-a practical guide. *J Exp Bot* **51**: 659-
24 668.
- 25 **Mhamdi A, Mauve C, Gouia H, Saindrenan P, Hodges M, Noctor G** (2010) Cytosolic NADP-
26 dependent isocitrate dehydrogenase contributes to redox homeostasis and the regulation of pathogen
27 responses in Arabidopsis leaves. *Plant Cell Env* **33**: 1112-1123
- 28 **Mitra SK, Gantt JA, Ruby JF, Clouse SD, Goshe MB** (2007) Membrane proteomic analysis
29 of *Arabidopsis thaliana* using alternative solubilization techniques. *J. Proteome Res.* **6**: 1933-1950
- 30 **Pou de Crescenzo M-A, Gallais S, Léon A, Laval-Martin DL** (2001) Tween-20 activates and
31 solubilizes the mitochondrial membrane-bound, calmodulin dependent NAD⁺ kinase of *Avena sativa* L.
32 *J Membr Biol* **182**: 135–146
- 33 **Pugin A, Frachisse JM, Tavernier E, Bligny R, Gout E, Douce R, Guern J** (1997) Early events
34 induced by the elicitor cryptogein in tobacco cells: involvement of a plasma membrane NADPH oxidase
35 and activation of glycolysis and the pentose phosphate pathway. *Plant Cell* **9**: 2077-2091
- 36 **Rhoads AR, Friedberg F** (1997) Sequence motifs for calmodulin recognition. *The FASEB*
37 *Journal* **11**: 331–340
- 38 **Sauer A, Robinson DG** (1985) Calmodulin dependent NAD-kinase is associated with both the
39 outer and inner mitochondrial membranes in maize roots. *Planta* **166**: 227-233
- 40 **Scharte J, Schön H, Tjaden Z, Weis E, von Schaewen A** (2009) Isoenzyme replacement of
41 glucose-6-phosphate dehydrogenase in the cytosol improves stress tolerance in plants. *Proc Natl Acad*
42 *Sci U S A* **106**: 8061-8066

1 **Schwarzländer M, Logan DC, Fricker MD, Sweetlove LJ** (2011) The circularly permuted
2 yellow fluorescent protein cpYFP that has been used as a superoxide probe is highly responsive to pH
3 but not superoxide in mitochondria: implications for the existence of superoxide 'flashes'. *Biochem J.*
4 **437**: 381-7

5 **Torres MA, Dangl JL** (2005) Functions of the respiratory burst oxidase in biotic interactions,
6 abiotic stress and development. *Curr Opin Plant Biol* **8**: 397-403

7 **Turner WL, Waller JC, Vanderbeld B, Snedden WA** (2004). Cloning and characterization of
8 two NAD kinases from Arabidopsis. Identification of a calmodulin binding isoform. *Plant Physiol* **135**:
9 1243-1255

10 **Wagner S, Behera S, De Bortoli S, Logan DC, Fuchs P, Carraretto L, Teardo E, Cendron**
11 **L, Nietzel T, Füßl M, Doccua FG, Navazio L, Fricker MD, Van Aken O, Finkemeier I, Meyer AJ,**
12 **Szabò I, Costa A, Schwarzländer M** (2015) The EF-hand Ca²⁺ binding protein MICU choreographs
13 mitochondrial Ca²⁺ dynamics in Arabidopsis. *The Plant Cell* **27**: 3190–3212

14

15 **Figures legends**

16 **Figure 1.** Biochemical properties of a CaM-dependent NAD⁺ kinase identified in Arabidopsis. (A)
17 NAD⁺ kinase activity measured in an *E. coli* extract expressing an empty pET28b(+) and an *E. coli*
18 extract expressing At1g04280. Spikes correspond to the moments of addition of glucose 6-phosphate
19 dehydrogenase (G6PDH), Ca²⁺, AtCaM1, and *E. coli* extracts (10 µg). (B) NAD⁺ kinase activity in an
20 *E. coli* bacterial extract expressing At1g04280. Ca²⁺, AtCaM1 and EGTA were added at different times,
21 as indicated in the graph. (C) Schematic representation of the NADKc primary sequence and comparison
22 with previously known NAD⁺ kinases. Yellow: zeta-toxin domain (InterPro Homologous superfamily:
23 IPR010488); black: N-terminal region with putative organelle target sequence; red: putative conserved
24 Type A 1-8-14 CaM-binding site (detailed below the scheme); orange: Walker A motif (ATP-binding
25 site); blue: NAD⁺ kinase domain (InterPro Homologous Superfamily: IPR016064); red/grey: N-terminal
26 sequence expected to contain a CaM-binding site according to Love et al, 2015. Sequences used for
27 comparison (UniProt): *E. coli* NAD⁺ kinase: P0A7B3; *A. thaliana* NAD⁺ kinases: AtNADK1: Q56YN3;
28 AtNADK2: Q9C5W3; AtNADK3: Q500Y9; *Strongylocentrotus purpuratus* NAD⁺ kinase-2 (sea urchin
29 CaM-dependent NAD⁺ kinase, Love et al., 2015): C3RSF7. (D) Affinity of NADKc recombinant protein
30 for AtCaM1: Activity of the purified NADKc recombinant protein after denaturation in urea and
31 subsequent refolding was measured in the presence of 50 µM Ca²⁺ and as a function of [AtCaM1].
32 Experiments were performed in triplicate and data shown are from one representative experiment.

1 Binding data were analysed assuming tight binding. K_d value for AtCaM1 binding varied from 0.6 to 1
2 nM. (E) Inhibition of NADKc activity by competition with the putative CaM-binding site (black dots).
3 Black squares correspond to results obtained with a negative control peptide, which does not bind
4 AtCaM1.

5 **Figure 2.** Analysis of submitochondrial localization of NADK_{C_{Nter}}-YFP. (A to C) Confocal laser
6 scanning microscopy images from stomata guard cells of a representative Arabidopsis seedling stably
7 expressing NADK_{C_{Nter}}-YFP. Scale bar = 5 μ m. (D to E) Higher magnification of the region of interest
8 shown in A to C (white squares). Scale bar = 1 μ m. (A, D) YFP fluorescence in green; (B, E) chlorophyll
9 fluorescence in blue; (C, F) merge between YFP and chlorophyll fluorescences. (G to I) Confocal laser
10 scanning microscopy images from root tip cells of a representative Arabidopsis seedling stably
11 expressing NADK_{C_{Nter}}-YFP and stained with the mitochondrial matrix marker TMRM. Scale bar = 1
12 μ m. (J to L) Confocal laser scanning microscopy images from root tip cells of a representative
13 Arabidopsis seedling stably expressing NMT-GFP and stained with the mitochondrial matrix marker
14 TMRM. Scale bar = 1 μ m. (M to O) Confocal laser scanning microscopy images from root tip cells of
15 a representative Arabidopsis seedling stably expressing MT-cpYFP and stained with the mitochondrial
16 matrix marker TMRM. Scale bar = 1 μ m. (G, M) YFP fluorescence in green; (J) GFP fluorescence in
17 green; (H, K and N) TMRM fluorescence in magenta; (I, L and O) merge between YFP/GFP and TMRM
18 fluorescences. NMT1-GFP and MT-cpYFP were used as markers for the mitochondrial outer
19 mitochondrial membrane (OMM) and matrix, respectively. (P to R) Normalized pixel intensity
20 distributions in the YFP and TMRM fluorescence channels plotted centrally across three individual
21 mitochondria of a seedling expressing the NADK_{C_{Nter}}-YFP.

22 **Figure 3.** The CaM/Ca²⁺-dependent NAD⁺ kinase activity of Arabidopsis seedlings is absent in *nadkc*
23 mutants. (A) schematic representation of the NADKc gene and position of the T-DNA insertions in the
24 *nadkc-1* and *nadkc-2* mutant lines. (B) NADKc transcript levels in Col-0 and *nadkc*-mutant seedlings.
25 Levels are expressed relative to GAPDH. Data shown correspond to mean +/- s.d., n=3. (C) NAD⁺
26 kinase activity measured in Col-0 and *nadkc* mutant plants (7-day-old whole plantlets), in the presence
27 of the CaM inhibitor TFP (40 μ M) or AtCaM1 (250 nM) and Ca²⁺ (0.5 mM). Values correspond to the
28 average of four replicates. (D) NAD⁺ kinase activity measured in Col-0 and mutant plants complemented

1 with NADKc gene (*nadkc-1_NADKc-1* and *nadkc-1_NADKc-2*) in 7-day-old whole plantlets, in the
2 presence of the CaM inhibitor TFP (40 μ M) or of AtCaM1 (250 nM) and Ca²⁺ (0.5 mM). (E) NAD(P)⁺
3 and NAD(P)H concentrations in 7-day-old seedlings exposed (flg22, 1 μ M) or unexposed (H₂O) for 12
4 min. to the bacterial elicitor flagellin22. (80-100 mg of tissue per measure, data shown correspond to
5 mean +/- s.e.m. for 3 biological replicates). (F) Flg22 (1 μ M)-induced oxidative burst in 7-day-old Col-
6 0 and *nadkc* mutant seedlings (30 plantlets per well, data shown correspond to mean +/- s.d. for 4 wells).
7 (G) Flg22 (1 μ M)-induced oxidative burst in Col-0, *nadkc-1* mutant and mutant plants complemented
8 with NADKc gene (*nadkc-1_NADKc-1* and *nadkc-1_NADKc-2*); 7-day-old seedlings, 30 plantlets per
9 well. Data shown correspond to mean +/- s.d. for 4 wells. Asterisks indicate a significant difference
10 between two conditions based on a Welch's t test (*p < 0.05; ***p < 0.001).

11 **Figure 4.** Hypothetical model of the role of CaM/Ca²⁺-dependent NADKc in sustaining the flg22-
12 induced oxidative burst in Arabidopsis seedlings. Numbers refer to known sequential events; red
13 numbers highlight events related to NADKc activation: 1. binding of Flg22 elicitor to the Fls2 receptor
14 (Sun et al., 2013); 2. activation of proton efflux and Ca²⁺ influx; 3a. Ca²⁺-dependent activation of CDPKs
15 and CIPK/CBLs that phosphorylate RBOH proteins; 3b. Ca²⁺ binding to RBOH proteins; 3c. Ca²⁺
16 binding to CaM, leading to CaM structural modification and formation of the CaM/NADKc complex;
17 4. activation of NADP⁺ production by NADKc; 5. increased flux in the oxidative pentose phosphate
18 pathway (OPPP), leading to a higher availability of NADPH; 6. production of the extracellular oxidative
19 burst by NADPH oxidases (RBOH proteins).

20 **Table 1.** NADKc kinetic parameters.

21 **Table 2.** Comparison of CaM-dependent NADK activity in different photosynthetic organisms. NADK
22 activity (nmol·h⁻¹·mg⁻¹ protein) was measured in soluble protein extracts from *Arabidopsis thaliana*,
23 *Marchantia polymorpha*, *Klebsormidium flaccidum* and *Chlamydomonas reinhardtii* as detailed in
24 Methods. Activities are expressed in nmol/h/mg protein. ^aNADK activity measured in the presence of
25 CaM/Ca²⁺ represents CaM-independent plus CaM-dependent activity; ^bNADK activity measured in the
26 presence of trifluoroperazine (CaM inhibitor) represents CaM-independent NADK activity. ^cCaM/Ca²⁺-
27 dependent activity is the difference between total NADK activity and CaM/Ca²⁺-independent activity.

1 NADK activity in *C. reinhardtii* is independent on CaM/Ca²⁺ (the difference is within experimental
2 error).

3 **Supplemental Material and Methods**

4 **Partial purification of native NADKc**

5 To purify native CaM-dependent NAD⁺ kinase, Col-0 Arabidopsis plants seeds were sterilized, sown in
6 Murashige and Skoog (Murashige and Skoog, 1962) liquid medium (2.2 g L⁻¹) supplemented with 0.5 g
7 L⁻¹ sucrose and grown under continuous light (60 μE) in 250-mL flasks and under agitation (125 rpm).
8 Seven-day-old plants were rinsed with water, frozen in liquid nitrogen and ground with a mortar and
9 pestle. The powder was suspended in Buffer A (50 mM Tris-HCl pH 7.5, 400 mM KCl, 3 mM MgCl₂,
10 1 mM EGTA, 0.5 mM EDTA, 1 mM DTT, 1 mM NAD⁺, 10 μM leupeptine, 10 μM E64, 1 mM PMSF,
11 1 mM benzamidine and 5 mM ε-aminocaproic acid). The crude extract was centrifuged (15,000 g, 30
12 min, 4 °C) and the recovered soluble protein extract (432 mg, 72 mL, 0.74 μmol h⁻¹ mg⁻¹) was
13 precipitated with 50% ammonium sulfate (1 h, 4 °C) and centrifuged (20,000 g, 20 min). The protein
14 pellet was then suspended in 32 mL Buffer A (30 mL, 270 mg, 1.1 μmol h⁻¹ mg⁻¹) and loaded onto a
15 DEAE column (60 mL resin) equilibrated with Buffer A. AtCaM1/Ca²⁺-dependent NADK activity was
16 detected in the flow-through (120 mL, 84 mg, 1.8 μmol h⁻¹ mg⁻¹). NaCl (3.5 M) was added to this
17 fraction, and the protein solution was loaded onto a Butyl-Sepharose column (12 mL resin) equilibrated
18 with Buffer B - NaCl (50 mM Tris-HCl pH 7.0, 3.5 M NaCl, 100 mM KCl, 3 mM MgCl₂, 1 mM DTT).
19 Elution was performed by applying a linear gradient (60 mL) from 0 to 100% Buffer B-ethane diol (50
20 mM Tris-HCl pH 7.5, 30% ethane diol (v/v), 100 mM KCl, 3 mM MgCl₂, 1 mM DTT). Eluted fractions
21 containing AtCaM1/Ca²⁺-dependent NADK activity were supplemented with 1 mM NAD⁺ and
22 immediately frozen. Fractions were pooled (5.6 mg, 2.32 μmol h⁻¹ mg⁻¹, 8 mL) before loading onto a 1-
23 mL CaM-Sepharose column (Stratagen) equilibrated with buffer C (50 mM Tris pH 7.5, 10% (v/v)
24 glycerol, 1 mM DTT, 2 mM CaCl₂). The column was washed with 10 volumes Buffer C supplemented
25 with 500 mM NaCl. Bound proteins were then eluted with 50 mM Tris pH 7.5, 10% (v/v) glycerol, 1
26 mM DTT and 5 mM EGTA. The fraction with highest activity (3 μg, 100 μl, 577 μmol h⁻¹ mg⁻¹) was
27 used for LC-MS/MS analyses (Fig. S1).

1 **Mass spectrometry-based proteomic analyses**

2 Proteins from the eluate and flow-through fractions were stacked by performing a very short run on an
3 SDS-PAGE gel (NuPAGE 4-12%, ThermoFisher Scientific). Proteins were revealed by staining with
4 Coomassie blue (R250, Bio-Rad), and submitted to in-gel digestion using modified trypsin (Promega,
5 sequencing grade), as previously described (Casabona et al., 2013).

6 Resulting peptides were analyzed by online nanoLC-MS/MS (UltiMate 3000 and LTQ23 Orbitrap Velos
7 Pro, Thermo Scientific). Briefly, peptides were sampled on a 300 μm x 5 mm PepMap C18 precolumn
8 and separated on a 75 μm x 250 mm C18 column (PepMap, Thermo Scientific). MS and MS/MS data
9 were acquired using Xcalibur (Thermo Scientific). Peptides and proteins were identified using Mascot
10 (version 2.6), performing concomitant searches against Uniprot (*A. thaliana* taxonomy), the classical
11 contaminants database (in-house) and the corresponding reversed databases. Proline software
12 (<http://proline.profiroteomics.fr>) was used to filter the results (conservation of rank 1 peptides, peptide
13 identification FDR < 1% as calculated on peptide scores using the reverse database strategy, minimum
14 peptide score of 25, and minimum of one specific peptide identified per protein group). Results from
15 individual samples were compiled, and grouped before comparing protein groups from different
16 samples. Proteins were considered to be enriched in the eluate if they were identified only in this sample
17 with a minimum of five specific spectral counts, or if they were enriched at least 10-fold in this sample
18 compared to flow-through sample. Relative quantification was performed on the basis of specific
19 spectral counts.

20 **Recombinant protein expression and purification**

21 Full-length At1g04280 cDNA was amplified by PCR from a pYES cDNA library (Elledge et al., 1991)
22 using the primers listed in Supplemental Table S2. The PCR products digested by Nde I and Xho I were
23 ligated into a pet28b(+) vector digested by the same enzymes to produce the constructs named pet28(b)-
24 6HIS-NADKc and pet28(b)-6HIS- Δ 38NADKc. The proteins were produced from these constructs with
25 a 22-amino-acid N-terminal His-tag.

1 Rosetta2-competent cells were transformed by one or the other of these two constructs and grown at 37
2 °C in the presence of Chloramphenicol (34 µg.mL⁻¹) and Kanamycin (50 µg.mL⁻¹) until Abs at 600 nm
3 reached 0.6. IPTG (0.4 mM) was added, and growth was continued at 20 °C for 15 h. Bacteria were
4 pelleted, suspended in Buffer D (50 mM HEPES pH 7.8, 500 mM KCl, 10% (v/v) glycerol, 50 mM L-
5 arginine, 50 mM L-glutamate, 1 mM NAD⁺) supplemented with 1 mM benzamidine and 5 mM ε-
6 aminocaproic acid, 1 mM β-mercaptoethanol, and lysed by sonication. Insoluble material was removed
7 by centrifugation (15,000 g, 20 min, 4 °C), and soluble proteins were recovered. A much higher
8 production level and higher activity were obtained with the 6HIS-Δ38-NADKc construct, therefore
9 further work was performed with this protein. The protein extract (30 mL, 11.3 mg mL⁻¹) was loaded
10 onto a Ni-NTA Sepharose column (3 mL resin). After washing with buffer D supplemented with 50 mM
11 imidazole (15 mL), the recombinant protein was eluted in buffer A supplemented with 250 mM
12 imidazole. The imidazole concentration was reduced to 5 mM by protein-concentration cycles followed
13 by dilution in buffer A. Pooled fractions containing NADKc activity were concentrated on 10K
14 Vivascience concentrators, aliquoted, frozen in liquid N₂ and stored at -80 °C. After this first purification
15 step, the protein fraction still contained small amounts of contaminating proteins. To improve
16 purification, Ni-NTA-Sepharose fractions (2 mg, 2.2 mL) were denatured in 8 M urea and purified on
17 Ni-NTA Sepharose under denaturing conditions (6 M urea). After washing with 15 mL buffer E (25
18 mM Tris-Cl pH 8.0, 500 mM NaCl, 5 mM β-mercaptoethanol, 6 M urea) supplemented with 50 mM
19 imidazole, the pure denatured protein was eluted in buffer E supplemented with 250 mM imidazole. The
20 denatured protein (0.3 mL, 0.3 mg, lane 4, Fig. S4) was then refolded by drop-by-drop dilution in 15
21 mL buffer D supplemented with 1 mM DTT. The refolding reaction was performed with mixing and at
22 room temperature. The highly purified protein (lane 5, Fig. S4) was then concentrated as described
23 above, aliquoted, frozen in liquid nitrogen and stored at -80 °C.

24 *A. thaliana* Calmodulin 1 (AtCaM1, At5g37780) was purified as previously described (Dell'Aglio et al.,
25 2013a).

26 Proteins were quantified by the Bradford method, using bovine γ-globulin as a standard or, for purified
27 proteins, by measuring A_{205nm} (Scopes, 1974). CaM-binding peptide

1 (QKVPKDKDFVMAATRQKQRFERVTKDLKVKR) was synthesized by Smart Bioscience (France).

2 The control peptide sequence was VKDTELAKKVWDFSTKLTDS (Dell'Aglio, 2013^b).

3 **Activity measurements**

4 NADK activity in extracts prepared from Col-0 *A. thaliana* plants, *K. flaccidum*, *M. polymorpha* and *C.*
5 *reinhardtii* was measured at 25 °C as previously described (Turner et al., 2004) in the presence of a CaM
6 inhibitor (trifluoroperazine, 50 μM) or in the presence of AtCaM1 (1 μM) and Ca²⁺ (500 μM) .
7 Recombinant NADKc activity was measured in thermostatic cuvettes (25 °C) with 20 nM enzyme in
8 the presence of 50 mM HEPES-KOH pH 7.8, 5 mM glucose-6-phosphate, 10 mM MgCl₂ and variable
9 concentrations of NAD⁺ and ATP (or other nucleotide), 30 mU of glucose-6-phosphate dehydrogenase
10 from baker's yeast and, where indicated in the figure legends, 50 μM Ca²⁺ and/or AtCaM1. NADPH
11 production was detected by monitoring absorbance at 340 nm ($\epsilon_{340\text{ nm}} = 6250\text{ M}^{-1}\text{ s}^{-1}$). Kinetic data
12 reported in Table 1 were calculated by fitting enzymatic data to the appropriate theoretical equations
13 using the Kaleidagraph program (Synergy Software, Reading, PA, USA). Tight binding of AtCaM1
14 onto NADKc was fitted using Eqn. 1:

$$15 \quad v/[E]_0 = k_{cat} \frac{([CaM] + k_d + [E]_0) - \sqrt{([CaM] + k_d + [E]_0)^2 - 4 * k_d * [E]_0}}{2[E]_0}$$

16 (Eqn.1)

17 where k_{cat} is the catalytic constant for NADKc, $[CaM]$ is the total CaM concentration, k_d is the
18 dissociation constant for the interaction between CaM and NADKc, and $[E]_0$ is the total NADKc
19 concentration.

20 **Subcellular localization by confocal microscopy**

21 The N-ter of the protein (amino acids: 1-60) or the entire protein sequence was amplified by PCR from
22 pet28(b)-6HIS-NADKc using the primers listed in Supplemental Table S2. The amplified PCR products
23 were cloned into the Gateway-adapted vector pDONR211 by BP recombination, to produce
24 pDONR:NADKc_{Nter}, pDONR:NADKc and pDONR:NADKc_{STOP} constructs.

1 These vectors were then recombined with pB7YWG2,0 and pB7WGY2,0 vectors (Karimi et al., 2007),
2 respectively, to generate pB7YWG2:NADK_{C_{Nter}}-YFP, pB7YWG2:NADK_C-YFP and pB7WGY2:YFP-
3 NADK_C through the LR recombination reaction. All vectors were transformed into *Agrobacterium*
4 *tumefaciens* C58 and used for tobacco leaf infiltration.

5 Transient expression in *Nicotiana benthamiana* var. Xanthi was performed by infiltrating leaves with a
6 suspension of *A. tumefaciens* harboring pB7YWG2:NADK_{C_{Nter}}-YFP and RFP fused with the first 69
7 amino acids of ATP synthase subunit 9a mitochondrial marker (pSu9-RFP) (Michaud et al., 2014) or
8 pB7WGY2:YFP:NADK_C, and the silencing suppressor P19 protein.

9 Transformed samples were observed by confocal microscopy on a LSM 800 confocal microscope
10 equipped with a Plan-Apo 63X/1.4 oil DIC lens, two GaAsP detectors and one Airyscan detector. YFP
11 and RFP fluorophores were excited at 488 and 558 nm, respectively, and emission signals were
12 measured at 488-560 nm for YFP, and at 568-611 nm for RFP.

13 Stable expression in *Arabidopsis thaliana* seedlings was achieved by transforming the localization
14 vectors into *A. tumefaciens* C58, which was used for floral dipping transformation. Complemented lines
15 were screened based on their BASTA-resistance.

16 Confocal microscopy analyses of stable transgenic *Arabidopsis* seedlings root and shoot cells were
17 performed using a Nikon Eclipse Ti2 inverted microscope, equipped with a Nikon A1+ laser scanning
18 device (Nikon). Images were acquired by a CFI Apochromat TIRF 100XC, 1.49 N.A., oil immersion.
19 EGFP or YFP were excited with the 488 nm laser and the emission was collected at 525-550 nm. For
20 co-localization studies with Tetramethylrhodamine, Methyl Ester, Perchlorate (TMRM) seedlings were
21 dipped in the following solution: 10 mM MES, 5 mM KCl, 10 mM CaCl₂, pH 5.8 with TRIS-base
22 supplemented with 500 nM TMRM. TMRM was excited with the 561 nm laser and the emission was
23 collected at 570-620 nm. Chlorophyll was excited with the 488 nm laser and the emission was collected
24 at 663-738 nm. Pinhole was set to 0.6 (Figure 2A to F) or 0.8 (Figure 2G-O) airy unit and the images
25 were acquired using 2048 x 2048 pixels. Pixel intensities of the YFP and TMRM fluorescences were
26 extracted using FIJI software (<https://fiji.sc/>).

1 **Measurement of photosynthetic parameters**

2 Maximum quantum yield of photosystem II (F_v/F_m), relative electron transport rate (ETR) and non-
3 photochemical quenching (NPQ) were determined using a chlorophyll fluorescence imaging system
4 (SpeedzenIII, JbeamBio, France) $F_v/F_m: (F_m - F_o)/F_m$; $ETR = ((F_m' - F_s)/F_m')$; $NPQ = (F_m - F_m')/F_m'$;
5 where F_m = maximum fluorescence; F_o = minimum fluorescence; F_v = variable fluorescence ($F_v = F_m -$
6 F_o) in dark-adapted state (Maxwell and Johnson, 2000). F_m' , maximum fluorescence in the light; F_s ,
7 steady-state chlorophyll fluorescence. Plants were dark adapted for at least 30 minutes prior to
8 measurement.

9 **Mutant complementation**

10 To complement the SALK_006202 NADKc mutant line, the entire NADKc protein sequence was
11 amplified by PCR from pet28(b)-6HIS-NADKc using the primers listed in Supplemental Table S1. The
12 amplified PCR product was cloned into the Gateway-adapted vector pDONR211 by BP recombination,
13 thus generating pDONR:NADKcSTOP. This vector was then recombined with pB2GW7,0 (Karimi et
14 al., 2007) to generate pB2GW7:NADKc by the LR recombination reaction. This vector was transformed
15 into *A. tumefaciens* C58 and used for floral dipping transformation. Complemented lines were screened
16 based on their BASTA-resistance and AtCaM1/Ca²⁺- dependent NAD⁺ kinase activity.

17 Lines for which levels of AtCaM1/Ca²⁺-dependent NAD⁺ kinase activity were similar to wild-type
18 plants were further analyzed.

19 **NAD(P)⁺ measurements**

20 NAD(P)(H) cycling assays were adapted from Gibon and Larher (1997). All reagents were from Sigma.
21 *A. thaliana* plantlets were grown for seven days in continuous light (Benamar A, 2013) then challenged
22 for 12 min. with flg22 (1 μ M) as previously described (Bisceglia & Savatin, 2015). Seedlings were
23 harvested in pools of 80-100 mg each and immediately frozen in liquid nitrogen. Reduced and oxidised
24 forms were extracted with 100 mM NaOH and 100 mM HCl respectively, and heated at 95°C for 5 min.
25 After cooling down, tubes were centrifuged at 10,000 g for 10 min. Then 5 μ l of the supernatant were
26 transferred to flat bottom polystyrene microplates (Greiner), neutralised with 5 μ l of 100 mM HCl

1 (reduced forms) or 100 mM NaOH (oxidised forms), and 90 μ l of determination mix added. For NAD(H)
2 measurements, final concentrations of the reagents were 100 mM Tricine/KOH buffer, pH 9.0, 10 mM
3 $MgCl_2$, 8 mM EDTA, 1% v/v ethanol, 1 mM thiazolyl blue, 0.5 mM phenazine ethosulfate and 20
4 units·ml⁻¹ alcohol dehydrogenase (Merck). For NADP(H) measurements, final concentrations of the
5 reactants were 100 mM Tricine/KOH buffer, 10 mM $MgCl_2$, 8 mM EDTA, 5 mM glucose-6-phosphate,
6 1 mM thiazolyl blue, 0.5 mM phenazine ethosulfate and 10 units·ml⁻¹ glucose-6-phosphate
7 dehydrogenase grade I (Merck). Changes in absorbance were read at 570 nm in an MP96 reader
8 (SAFAS) until stabilised. For each coenzyme form and/or each microplate a standards curve ranging
9 from 0 to 40 pmol per well was used; blanks without enzyme were also recorded in order to subtract
10 interferences coming from the extracts. Results are expressed as the average obtained for 3 independent
11 extracts.

12 **Oxidative burst measurements**

13 *A. thaliana* plantlets were grown for 7 days in continuous light (Benamar et al., 2013) and immunity-
14 related accumulation of H₂O₂ following stimulation with flg22 (1 μ M) was analyzed as previously
15 described (Bisceglia & Savatin, 2015). The purity of the flg22 peptide (synthesized by GENECUST,
16 Boynes, France) was estimated at 96.14%. Luminescence measurements were performed with a
17 microplate reader SPARK 10M (TECAN) using 96-well microtiter plates (flat bottom, white, Greiner).
18 For each plant type, results are expressed as the average luminescence obtained for 4 wells (*i.e.*, 120
19 plantlets).

20 **Molecular Phylogenetic analysis by the Maximum Likelihood method**

21 Protein sequences of NADKc-like proteins were retrieved from the Phytozome website (Goodstein et
22 al., 2012), with some exceptions. The sequences of *U. mutabilis* and *C. braunii* were retrieved from the
23 ORCAE project website (Sterck et al., 2012) and those of *S. minuta*, *E. fimbriata*, *Mougeotia* sp. and
24 *Spirogyra* sp. were retrieved from the One KP project website (Matasci et al., 2014). The evolutionary
25 history of NADKc was inferred by using the Maximum Likelihood method, based on the JTT matrix-
26 based model (Jones et al., 1992). The tree with the highest log-likelihood (-31386.44) is shown. The

1 percentage of trees produced in which the associated taxa clustered together is shown next to the
2 branches. Initial tree(s) for the heuristic search were obtained automatically by applying Neighbor-Join
3 and BioNJ algorithms to a matrix of pairwise distances estimated using a JTT model, and then selecting
4 the topology with the highest log-likelihood value. A discrete Gamma distribution was used to model
5 evolutionary rate differences between sites (5 categories (+G, parameter = 0.9891)). The tree is drawn
6 to scale, with branch lengths based on the number of substitutions per site. The analysis involved 45
7 amino acid sequences. There were a total of 1196 positions in the final dataset. Evolutionary analyses
8 were performed in MEGA7 (Kumar et al., 2016).

9

10 Supplemental references

11 **Benamar A, Pierart A, Baecker V, Avelange-Macherel M, Rolland A, Gaudichon S, di Gioia**
12 **L, Macherel, D** (2013) Simple system using natural mineral water for high-throughput phenotyping of
13 *Arabidopsis thaliana* seedlings in liquid culture. *International Journal of High Throughput Screening* **4**:
14 1-15

15 **Bisceglia NG, Gravino M, Savatin DV** (2015) Luminol-based Assay for Detection of Immunity
16 Elicitor-induced Hydrogen Peroxide Production in *Arabidopsis thaliana* Leaves. *BioProtocols* **5**: 1-7

17 **Casabona M, Vandenbrouck Y, Attree I, and Couté Y** (2013) Proteomic characterization of
18 *Pseudomonas aeruginosa* PAO1 inner membrane. *Proteomics* **13**: 2419-2423

19 **Dell'Aglio E, Giustini C, Salvi D, Brugière S, Delpierre F, Moyet L, Baudet M, Seigneurin-**
20 **Berny D, Matringe M, Ferro M, et al** (2013^a) Complementary biochemical approaches applied to the
21 identification of plastidial calmodulin-binding proteins. *Mol Biosyst* **9**: 1234-1248

22 **Dell'Aglio E** (2013^b) The regulation of plastidial proteins by calmodulins. Université de Grenoble

23 **Elledge SJ, Mulligan JT, Ramer SW, Spottswood M, Davis RW** (1991) Lambda YES: a
24 multifunctional cDNA expression vector for the isolation of genes by complementation of yeast and
25 *Escherichia coli* mutations. *Proc Natl Acad Sci USA* **88**: 1731-1735

26 **Gibon Y, Larher F** (1997) Cycling assay for nicotinamide adenine dinucleotides: NaCl precipitation
27 and ethanol solubilization of the reduced tetrazolium. *Analytical Biochemistry* **251**: 153-157

28 **Goodstein DM, Shu SQ, Howson R, Neupane R, Hayes RD, Fazo J, Mitros T, Dirks W, Hellsten**
29 **U, Putnam N, et al** (2012) Phytozome: a comparative platform for green plant genomics. *Nucleic Acids*
30 *Research* **40**: D1178-D1186

31 **Jones D, Taylor W, Thornton J** (1992) The rapid generation of mutation data matrices from protein
32 sequences. *Comput Appl Biosci* **8**: 275-282

33 **Karimi M, Depicker A, Hilson P** (2007) Recombinational cloning with plant Gateway vectors.
34 *Plant Physiol* **145**: 1144-1154

35 **Kumar S, Stecher G, Tamura K** (2016) Molecular evolutionary genetics analysis version 7.0 for
36 bigger datasets. *Mol Biol Evol* **33**

37 **Matasci N, Hung LH, Yan ZX, Carpenter EJ, Wickett NJ, Mirarab S, Nguyen N, Warnow T,**
38 **Ayyampalayam S, Barker M, et al** (2014) Data access for the 1,000 Plants (1KP) project. *Gigascience*
39 **3**

40 **Michaud M, Ubrig E, Filleur S, Erhardt M, Ephritikhine G, Maréchal-Drouard L, Duchêne**
41 **A-M** (2014) Differential targeting of VDAC3 mRNA isoforms influences mitochondria morphology.
42 *Proc Natl Acad Sci USA* **111**: 8991-8996

43 **Murashige T, Skoog F** (1962) A revised medium for rapid growth of bioassays with tobacco tissue
44 culture. *Physiol Plant* **15**: 473-497

45 **Scopes RK** (1974) Measurement of protein by spectroscopy at 205 nm. *Anal. Biochem.* **59**: 277-282

1 Sun Y, Li L, Macho AP, Han Z, Hu Z, Zipfel C, Zhou JM, Chai J. (2013) Structural basis for
2 flg22-induced activation of the Arabidopsis FLS2-BAK1 immune complex. *Science* **342**: 624-8

3 Sterck L, Billiau K, Abeel T, Rouze P, van de Peer Y (2012) ORCAE: online resource for
4 community annotation of eukaryotes. *Nature Methods* **9**: 1041-1041

5 Turner WL, Waller JC, Vanderbeld B, Snedden WA (2004) Cloning and characterization of two
6 NAD kinases from Arabidopsis. Identification of a calmodulin binding isoform. *Plant Physiol* **135**:
7 1243-1255
8

9 Supplemental Figures Legend

10 **Supplementary Figure S1.** CaM-affinity purification of native CaM-dependent NAD⁺ kinase from
11 Arabidopsis plantlets. Proteins loaded and eluted from the CaM affinity chromatography column were
12 separated by SDS-PAGE and stained with silver nitrate. In the “Loaded fraction”, 24 µg in 38 µl were
13 loaded; in the washings and EGTA elution fractions, 38 µl of each fraction were loaded (concentration
14 not determined). Mass spectrometry-based proteomics was used to identify proteins strongly enriched
15 in the EGTA elution compared to the Ca²⁺-containing washing steps (Supplemental Table S1). Protein
16 bands analysed by mass spectrometry are included in red boxes.

17 **Supplementary Fig. S2.** Features of NADKc primary sequence and its homologues in other plant and
18 algae species. (A) putative CaM binding site (*A. thaliana* NADKc amino acids 167-200). Red residues
19 are those constituting the 1-5-8-14 motif. This domain is not conserved in *C. subellipsoidea*, *U. mutabilis*
20 and *S. minuta*. *A. thaliana*: *Arabidopsis thaliana*, *S. phallax*: *Sphagnum phallax*, *P. patens*:
21 *Physcomitrella patens*, *M. polymorpha*: *Marchantia polymorpha*, *S. mollendorffii*: *Selaginella*
22 *mollendorffii*, *S. lycopersicum*: *Solanum lycopersicum*, *G. max*: *Glycine max*, *M. truncatula*: *Medicago*
23 *truncatula*, *P. trichocarpa*: *Populus trichocarpa*, *M. acuminata*: *Musa acuminata*, *O. sativa*: *Oryza*
24 *sativa*, *B. distachyon*: *Brachypodium distachyon*, *S. italica*: *Setaria italica*, *Z. mays*: *Zea mays*, *C.*
25 *subellipsoidea*: *Coccomyxa subellipsoidea*, *U. mutabilis*: *Ulva mutabilis*, *S. minuta*: *Spirotaenia minuta*,
26 *K. flaccidum*: *Klebsormidium flaccidum*, *E. fimbriata*: *Entransia fimbriata*. (B) Walker A motif (in red,
27 residues characterizing the motif; *A. thaliana* NADKc amino acids 236-250). For gene references, see
28 the legend of Fig. S6.

29 **Supplementary Fig. S3.** Purification of recombinant NADKc produced in *E. coli*. 6HIS-Δ38NADKc
30 was purified as indicated in Material and Methods. Lane 1: Rosetta2 soluble extract transformed with
31 empty pET28a (40 µg); lane 2: Rosetta2 soluble extract transformed with pET28a6HIS-Δ38NADKc (40

1 μg); lane 3: Ni-NTA pool (10 μg); lane 4: urea-denatured 6HIS- Δ 38NADKc purified on Ni-NTA (10
2 μg); lane 5: refolded 6HIS- Δ 38NADKc (2 μg).

3 **Supplementary Fig. S4.** NADK_{cNter}-YFP associates with mitochondria in tobacco leaves.
4 Representative pictures of transiently transformed tobacco leaf cells. Left: YFP (green), Center: RFP
5 (red), and Right: merged fluorescence. The top row shows a representative image of tobacco cells co-
6 transformed with the NADK_{cNter}-YFP construct and a mitochondrial marker, pSu9-RFP. The middle
7 row shows a close-up of mitochondria from the lower right region of the images in the top row (white
8 boxes). White arrows indicate regions in which the YFP signal appears peripheral with respect to the
9 RFP signal. The bottom row shows a representative image of tobacco cells transformed with the YFP-
10 NADKc construct alone. The central image shows the background signal in the RFP channel. White
11 bars represent 2 μm in the upper and middle row, and 10 μm in the lower row.

12 **Supplementary Fig. S5.** Phenotype of *nadkc* mutants. (A) 21-day-old plants grown under long day
13 photoperiod (16 h light/8 h dark); (B) 28-day-old plants grown under short day photoperiod (8 h light/16
14 h dark). (C-E) Photosynthetic parameters in Col-0 and *nadkc* plants: (C) NPQ, (D) Fv/Fm and (E)
15 electron transport rate.

16 **Supplementary Fig. S6.** Phylogeny of NADKc. Maximum likelihood phylogenetic tree of NADKc-
17 like proteins in the following plant and algal species: *Arabidopsis thaliana* (*A. thaliana*), *Populus*
18 *trichocarpa* (*P. trichocarpa*), *Manihot esculenta* (*M. esculenta*), *Gossypium raimondii* (*G. raimondii*),
19 *Solanum lycopersicum* (*S. lycopersicum*), *Setaria italica* (*S. italica*), *Zea mays* (*Z. mays*), *Oryza sativa*
20 (*O. sativa*), *Brachypodium distachyon* (*B. distachyon*), *Musa acuminata* (*M. acuminata*), *Marchantia*
21 *polymorpha* (*M. polymorpha*), *Physcomitrella patens* (*P. patens*), *Sphagnum phallax* (*S. phallax*),
22 *Selaginella mollendorffii* (*S. mollendorffii*), *Klebsormidium flaccidum* (*K. flaccidum*), *Coccomyxa*
23 *subellipsoidea* (*C. subellipsoidea*), *Ulva mutabilis* (*U. mutabilis*), *Spirotaenia minuta* (*S. minuta*),
24 Mougeotia sp., Spirogyra sp. and *Entransia fimbriata* (*E. fimbriata*). Accession numbers: *A. thaliana*-1
25 (NADKc): At1g04280, *A. thaliana*-2: At1g06750, *A. thaliana*-3: At2g30630, *P. trichocarpa*-1:
26 Potri.008G162000, *P. trichocarpa*-2: Potri.002G043000, *P. trichocarpa*-3: Potri.005G220000, *P.*
27 *trichocarpa*-4: Potri.008G162400, *M. esculenta*-1: Manes.15G036900, *M. esculenta*-2:
28 Manes.03G168900, *M. esculenta*-3: Manes.01G200600, *M. esculenta*-4: Manes.05G086200, *G.*

1 *raimondii-1*: Gorai.011G171100, *G. raimondii-2*: Gorai.006G246600, *G. raimondii-3*:
2 Gorai.004G074100, *G. raimondii-4*: Gorai.013G104300, *S. lycopersicum-1*: Solyc06g053810, *S.*
3 *lycopersicum-2*: Solyc06g031670, *S. lycopersicum-3*: Solyc08g059750, *S. italica-1*: Seita.9G163700, *S.*
4 *italica-2*: Seita.3G185100, *S. italica-3*: Seita.5G337000, *Z. mays-1*: GRMZM2G070252, *Z. mays-2*:
5 GRMZM2G368410, *O. sativa-1*: Os03g43010, *O. sativa-2*: Os05g43300, *O. sativa-3*: Os01g56764, *B.*
6 *distachyon-1*: Bradi1g14307, *B. distachyon-2*: Bradi2g51490, *B. distachyon-3*: Bradi2g20400, *M.*
7 *acuminata-1*: SMUA_Achr5T03210, *M. acuminata-2*: GSMUA_Achr7T01560, *M. polymorpha*:
8 Mapoly0142s0012, *P. patens*: Pp3c2_3490V3, *S. phallax-1*: Sphallax0059s0037, *S. phallax-2*:
9 Sphallax0011s0002, *S. phallax-3*: Sphallax0120s0019, *S. mollendorffii-1*: scaffold 73427, *S.*
10 *mollendorffii-2*: scaffold 231175, *K. flaccidum*: kfl00274_0130, *C. subellipsoidea*: XP_005648203, *U.*
11 *mutabilis*: UM028_0076.1, *S. minuta*: NNHQ_2000691, *Mougeotia*: ZRMT_2002068, *Spirogyra*:
12 HAOX_2025158, *E. fimbriata*: BFIK_2025349. The tree is drawn to scale, with branch lengths
13 measured in the number of substitutions per site (scale bar in the bottom-left corner). The numbers at
14 the interior nodes are bootstrap percentages.

15 **Supplementary Table S1.** List of Arabidopsis proteins bound on CaM-affinity column in the presence
16 of Ca²⁺ and eluted by EGTA identified by mass-spectrometry.

17 **Supplementary Table S2.** Primers used in this study.

18

19

20 **Table 1: NADKc kinetic parameters**

Substrate varied	Constant substrate	K _M (μM)	k _{cat} (s ⁻¹)	k _{cat} /K _M (μM ⁻¹ .s ⁻¹)
ATP	NAD ⁺ (10 mM)	203(±30)	41(±2)	0.2
CTP	NAD ⁺ (10 mM)	283(±70)	42(±1)	0.15
GTP	NAD ⁺ (10 mM)	522(±135)	26(±1)	0.05
UTP	NAD ⁺ (10 mM)	207(±26)	29.5(±2)	0.14
NAD ⁺	ATP (8 mM)	147 (±17)	42(±2)	0.28
NADH ⁺	ATP (8 mM)	n.d.	n.d.	n.d.
NAAD ⁺	ATP (8 mM)	n.d.	n.d.	n.d.

21 n.d.: not detected

22

1

2 **Table 2: Comparison of CaM-dependent NADK activity in different photosynthetic organisms.**

	<i>A. thaliana</i>	<i>M. polymorpha</i>	<i>K. flaccidum</i>	<i>C. reinhardtii</i>
Total activity^a	31.2(±2.8)	6.9(±0.7)	5.8(±0.3)	24.6(±1.4)
CaM/Ca²⁺ - independent activity^b	1.0(±0.3)	1.0(±0.1)	1.8(±0.3)	29.7(±2.7)
CaM/Ca²⁺ - dependent activity^c	30.2	5.9	4.0	n.d.

3 n.d.: not detected.

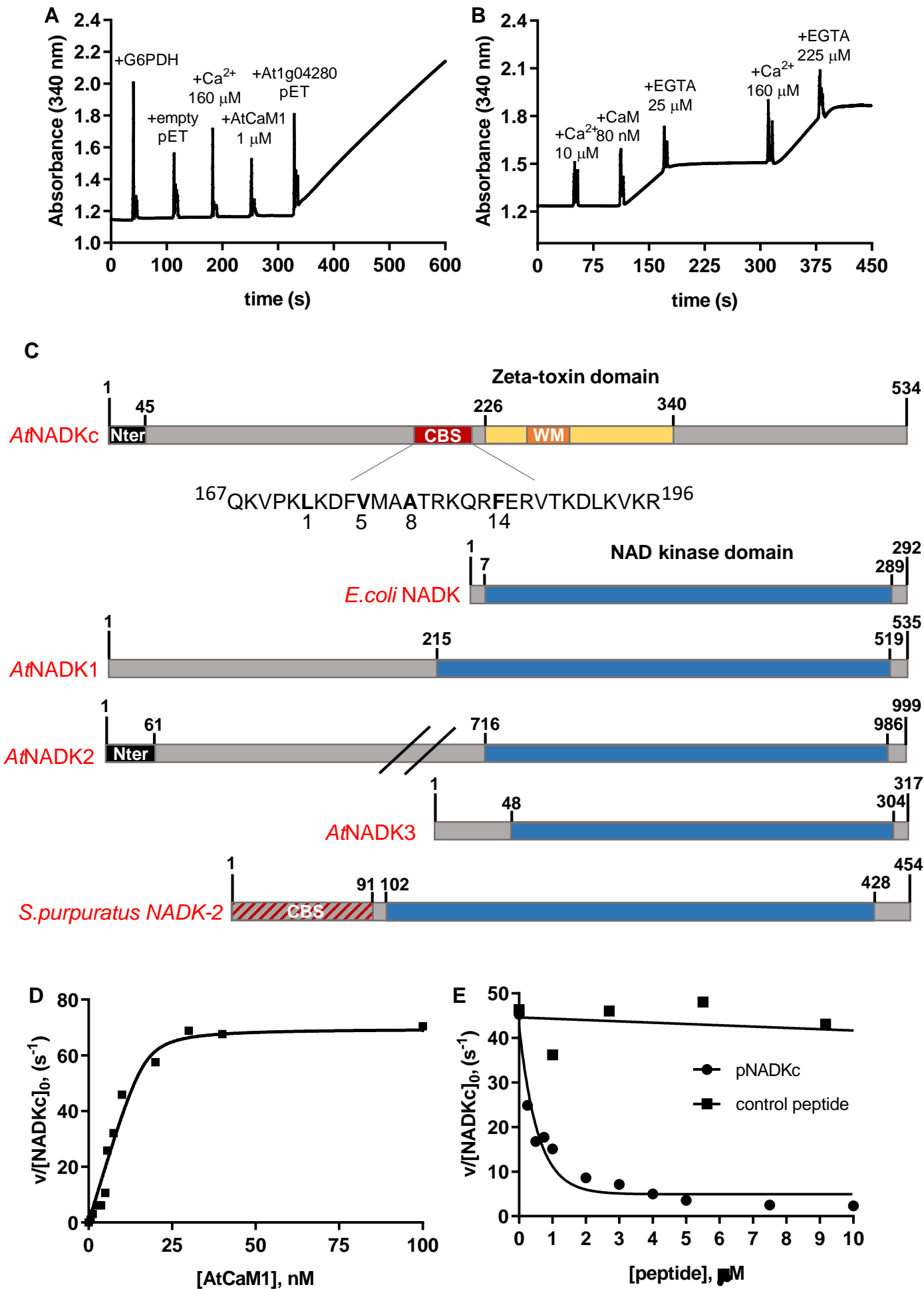
Figure 1

Figure 1. Biochemical properties of a CaM-dependent NAD⁺ kinase identified in Arabidopsis. (A) NAD⁺ kinase activity measured in an *E. coli* extract expressing an empty pET28b(+) and an *E. coli* extract expressing At1g04280. Spikes correspond to the moments of addition of glucose 6-phosphate dehydrogenase (G6PDH), Ca²⁺, AtCaM1, and *E. coli* extracts (10 μg). (B) NAD⁺ kinase activity in an *E. coli* bacterial extract expressing At1g04280. Ca²⁺, AtCaM1 and EGTA were added at different times, as indicated in the graph. (C) Schematic representation of the NADKc primary sequence and comparison with previously known NAD⁺ kinases. Yellow: zeta-toxin domain (InterPro Homologous superfamily: IPR010488); black: N-terminal region with putative organelle target sequence; red: putative conserved Type A 1-8-14 CaM-binding site (detailed below the scheme); orange: Walker A motif (ATP-binding site); blue: NAD⁺ kinase domain (InterPro Homologous Superfamily: IPR016064); red/grey: N-terminal sequence expected to contain a CaM-binding site according to Love et al, 2015. Sequences used for comparison (UniProt): *E. coli* NAD⁺ kinase: P0A7B3; *A. thaliana* NAD⁺ kinases: AtNADK1: Q56YN3; AtNADK2: Q9C5W3; AtNADK3: Q500Y9; *Strongylocentrotus purpuratus* NAD⁺ kinase-2 (sea urchin CaM-dependent NAD⁺ kinase, Love et al., 2015): C3RSF7. (D) Affinity of NADKc recombinant protein for AtCaM1: Activity of the purified NADKc recombinant protein after denaturation in urea and subsequent refolding was measured in the presence of 50 μM Ca²⁺ and as a function of [AtCaM1]. Experiments were performed in triplicate and data shown are from one representative experiment. Binding data were analysed assuming tight binding. K_d value for AtCaM1 binding varied from 0.6 to 1 nM. (E) Inhibition of NADKc activity by competition with the putative CaM-binding site (black dots). Black squares correspond to results obtained with a negative control peptide, which does not bind AtCaM1.

Figure 2

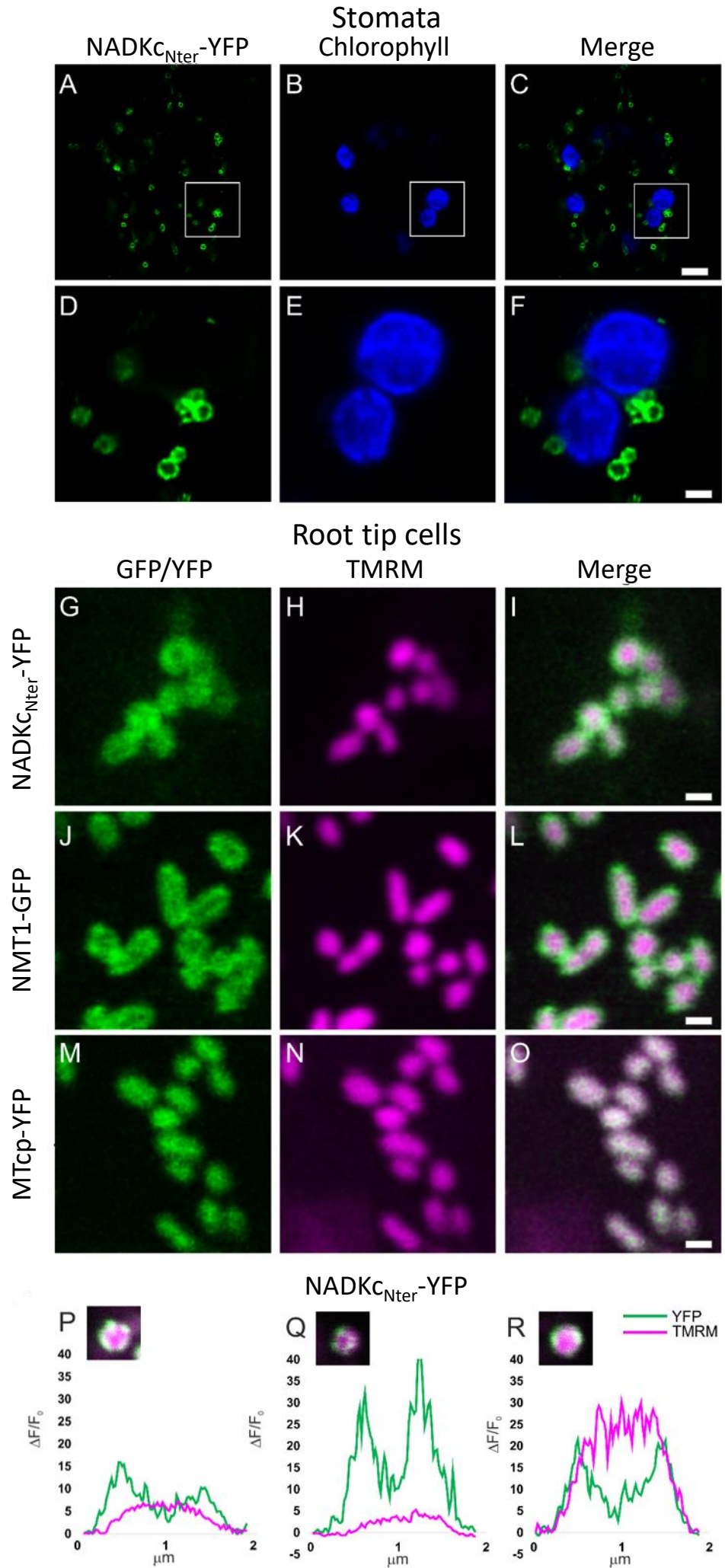


Figure 2. Analysis of submitochondrial localization of NADK_{C_{Nter}}-YFP. (A to C) Confocal laser scanning microscopy images from stomata guard cells of a representative Arabidopsis seedling stably expressing NADK_{C_{Nter}}-YFP. Scale bar = 5 μm. (D to E) Higher magnification of the region of interest shown in A to C (white squares). Scale bar = 1 μm. (A, D) YFP fluorescence in green; (B, E) chlorophyll fluorescence in blue; (C, F) merge between YFP and chlorophyll fluorescences. (G to I) Confocal laser scanning microscopy images from root tip cells of a representative Arabidopsis seedling stably expressing NADK_{C_{Nter}}-YFP and stained with the mitochondrial matrix marker TMRM. Scale bar = 1 μm. (J to L) Confocal laser scanning microscopy images from root tip cells of a representative Arabidopsis seedling stably expressing NMT-GFP and stained with the mitochondrial matrix marker TMRM. Scale bar = 1 μm. (M to O) Confocal laser scanning microscopy images from root tip cells of a representative Arabidopsis seedling stably expressing MT-cpYFP and stained with the mitochondrial matrix marker TMRM. Scale bar = 1 μm. (G, M) YFP fluorescence in green; (J) GFP fluorescence in green; (H, K and N) TMRM fluorescence in magenta; (I, L and O) merge between YFP/GFP and TMRM fluorescences. NMT1-GFP and MT-cpYFP were used as markers for the mitochondrial outer mitochondrial membrane (OMM) and matrix, respectively. (P to R) Normalized pixel intensity distributions in the YFP and TMRM fluorescence channels plotted centrally across three individual mitochondria of a seedling expressing the NADK_{C_{Nter}}-YFP.

Figure 3

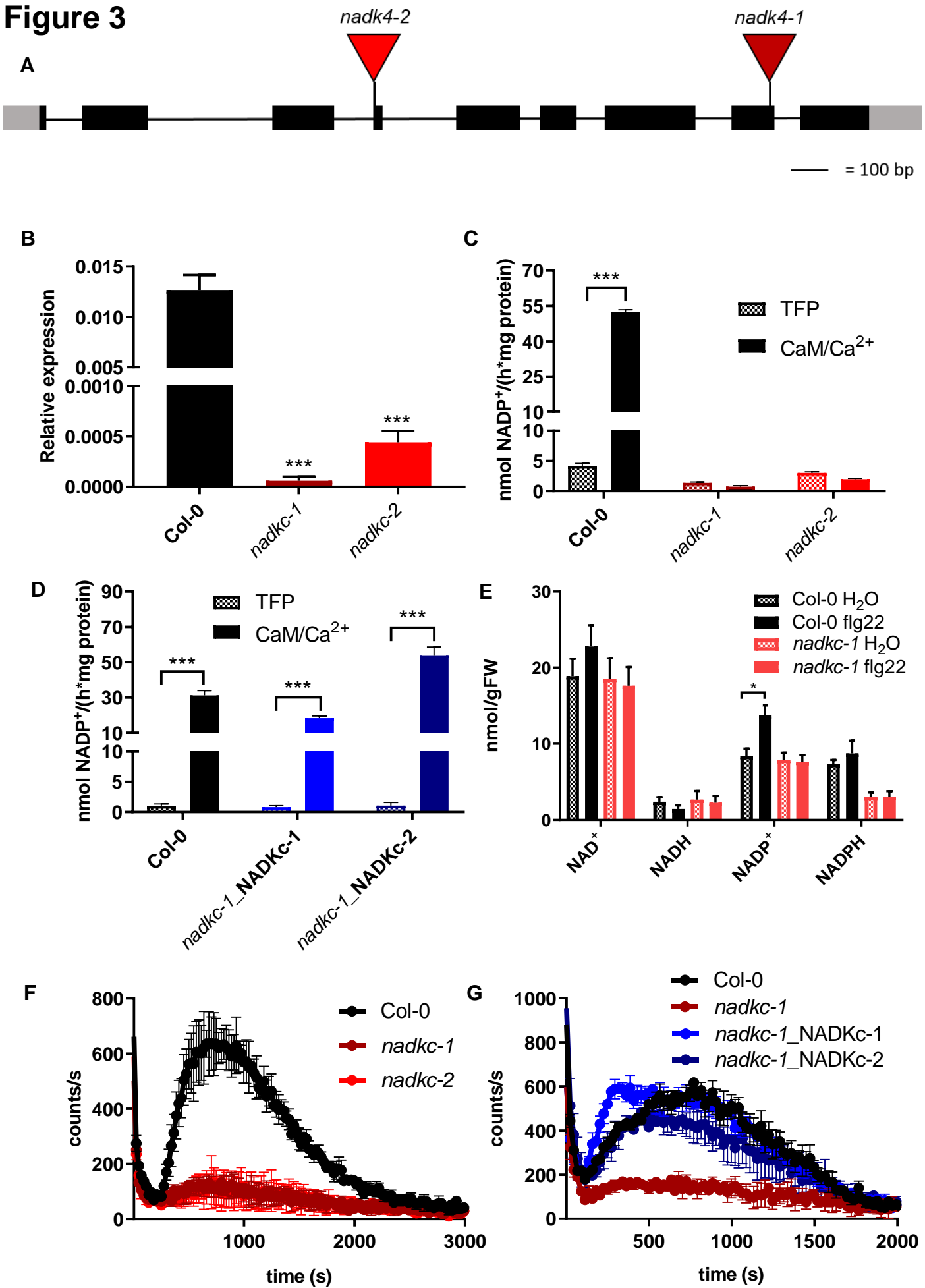


Figure 3. The CaM/Ca²⁺-dependent NAD⁺ kinase activity of Arabidopsis seedlings is absent in *nadkc* mutants. (A) schematic representation of the NADKc gene and position of the T-DNA insertions in the *nadkc-1* and *nadkc-2* mutant lines. (B) NADKc transcript levels in Col-0 and *nadkc*-mutant seedlings. Levels are expressed relative to GAPDH. Data shown correspond to mean +/- s.d., n=3. (C) NAD⁺ kinase activity measured in Col-0 and *nadkc* mutant plants (7-day-old whole plantlets), in the presence of the CaM inhibitor TFP (40 μM) or AtCaM1 (250 nM) and Ca²⁺ (0.5 mM). Values correspond to the average of four replicates. (D) NAD⁺ kinase activity measured in Col-0 and mutant plants complemented with NADKc gene (*nadkc-1_NADKc-1* and *nadkc-1_NADKc-2*) in 7-day-old whole plantlets, in the presence of the CaM inhibitor TFP (40 μM) or of AtCaM1 (250 nM) and Ca²⁺ (0.5 mM). (E) NAD(P)⁺ and NAD(P)H concentrations in 7-day-old seedlings exposed (flg22, 1 μM) or unexposed (H₂O) for 12 min. to the bacterial elicitor flagellin22. (80-100 mg of tissue per measure, data shown correspond to mean +/- s.e.m. for 3 biological replicates). (F) Flg22 (1 μM)-induced oxidative burst in 7-day-old Col-0 and *nadkc* mutant seedlings (30 plantlets per well, data shown correspond to mean +/- s.d. for 4 wells). (G) Flg22 (1 μM)-induced oxidative burst in Col-0, *nadkc-1* mutant and mutant plants complemented with NADKc gene (*nadkc-1_NADKc-1* and *nadkc-1_NADKc-2*); 7-day-old seedlings, 30 plantlets per well. Data shown correspond to mean +/- s.d. for 4 wells. Asterisks indicate a significant difference between two conditions based on a Welch's t test (*p < 0.05; ***p < 0.001).

Figure 4

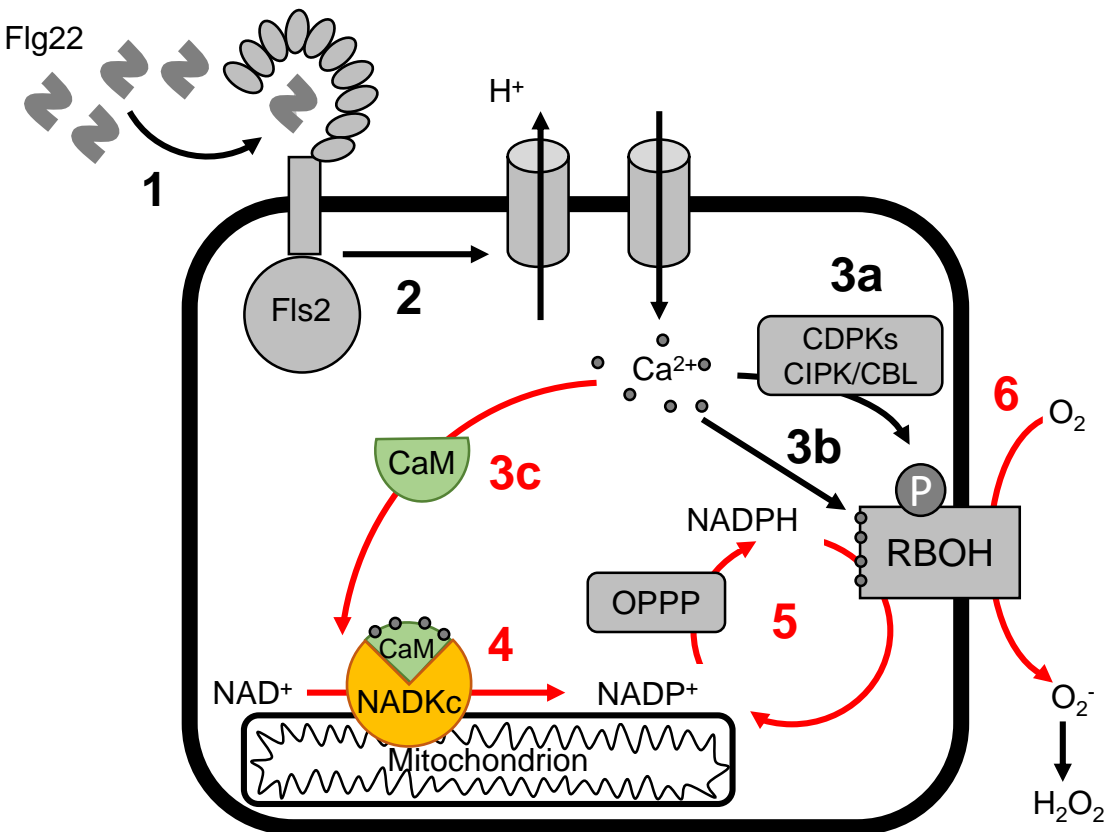
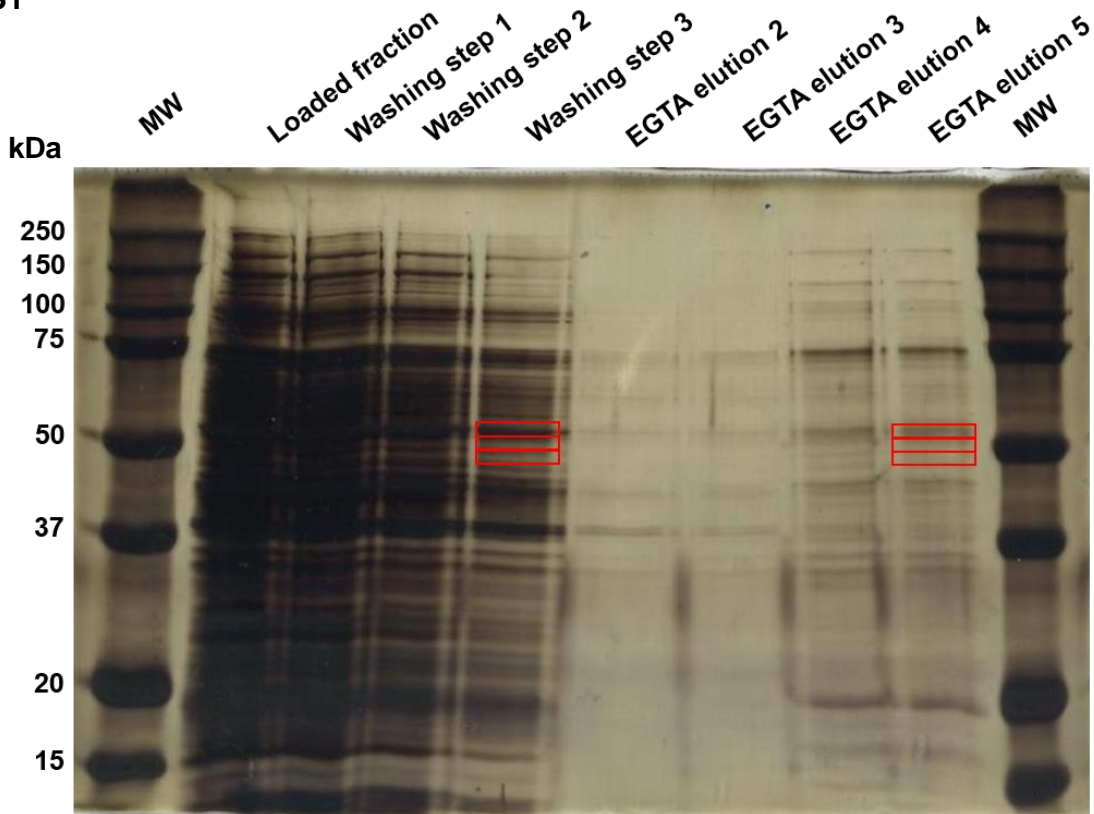


Figure 4. Hypothetical model of the role of CaM/Ca²⁺-dependent NADKc in sustaining the flg22-induced oxidative burst in Arabidopsis seedlings. Numbers refer to known sequential events; red numbers highlight events related to NADKc activation: 1. binding of Flg22 elicitor to the Fls2 receptor (Sun et al., 2013); 2. activation of proton efflux and Ca²⁺ influx; 3a. Ca²⁺-dependent activation of CDPKs and CIPK/CBLs that phosphorylate RBOH proteins; 3b. Ca²⁺ binding to RBOH proteins; 3c. Ca²⁺ binding to CaM, leading to CaM structural modification and formation of the CaM/NADKc complex; 4. activation of NADP⁺ production by NADKc; 5. increased flux in the oxidative pentose phosphate pathway (OPPP), leading to a higher availability of NADPH; 6. production of the extracellular oxidative burst by NADPH oxidases (RBOH proteins).

Figure S1



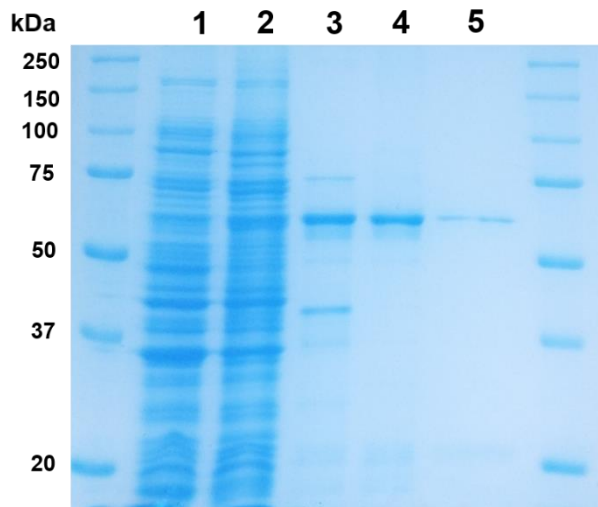
Supplemental Figure S1. CaM-affinity purification of native CaM-dependent NAD⁺ kinase from Arabidopsis plantlets. Proteins loaded and eluted from the CaM affinity chromatography column were separated by SDS-PAGE and stained with silver nitrate. In the “Loaded fraction”, 24 μ g in 38 μ l were loaded; in the washings and EGTA elution fractions, 38 μ l of each fraction were loaded (concentration not determined). Mass spectrometry-based proteomics was used to identify proteins strongly enriched in the EGTA elution compared to the Ca²⁺-containing washing steps (Supplemental Table S1). Protein bands analysed by mass spectrometry are included in red boxes.

Figure S2**A****Predicted CaM-binding site****B****Walker A motif**

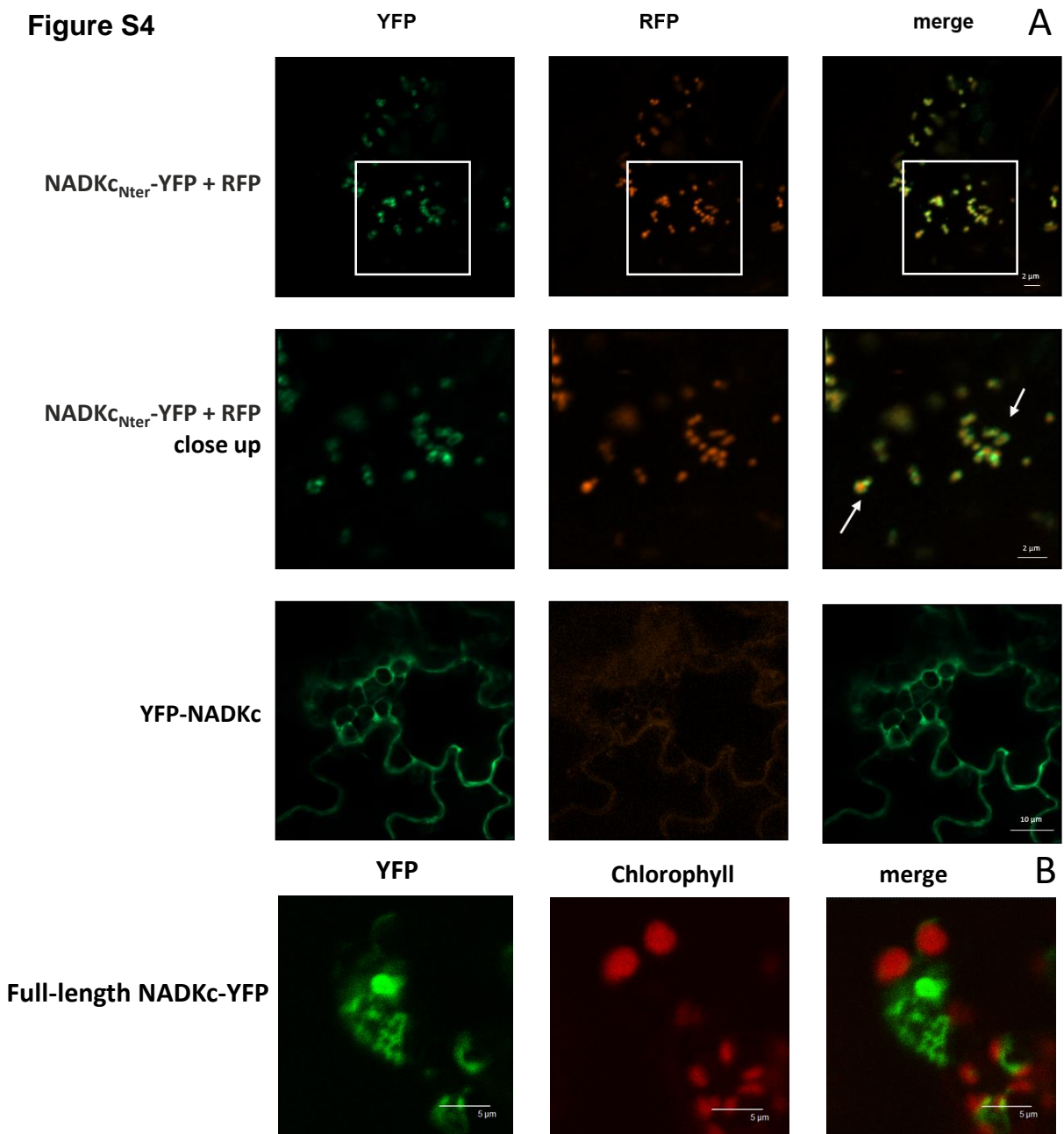
<i>A. thaliana-1</i> (At1g04280 - NADKc)	167	QKVPK L KDFVMA A TRKQ R FERVTKDLKV K R	196	236	MGGGMGAG K STVL K D	250
Plants						
<i>S. phfallax-1</i>		--QK R L R KAV L LA T RPQ R I E RV L K C L K TK R			I G GGMGAG K STV V Q E	
<i>P. patens</i>		--E K K L H K AV L C A L K KQ R Y E AV L K S L S TK R			I G GGMGAG K ST I V K E	
<i>M. polymorpha</i>		-Q K R S L K KAV L S A TRKQ R Y Q RV M Q D L K TK R			I G GGMGAG K ST V V K E	
<i>S. mollendorffii-1</i>		----N L R S I V MA A TRK H R F Q R AM Q T L K A K R			M G GGMGAG K ST V L K D	
<i>S. lycopersicum-1</i>		--Q K R L K D L V LA A TRKQ R F E K I T K D L K V T R			M G GGMGAG K ST V L K D	
<i>G. max-1</i>		-Q K K K L K G I L L A A T R E Q R F DR V T K N L K V T R			M G GGMGAG K ST V L K D	
<i>M. esculenta-1</i>		-K R H K L K D V V L A A TRKQ R F ER V N K E L K V T R			M G GGMGAG K ST V I K D	
<i>P. trichocarpa-1</i>		-K K P K L K G I V M A A TRKQ R F ER V T K N L K V T R			M G GGMGAG K ST V T K D	
<i>M. acuminata-1</i>		-Q K M K L K N F V M E A TR K L R F ER V T K D L K V T R			M G GGMGAG K ST V L K E	
<i>O. sativa-1</i>		A S K K K L R N L V L E A T R K Q R F ER V T R D L K V T R			M G GGMGAG K ST V L K E	
<i>B. distachyon-1</i>		-T R K K L R N L V L E A T R K Q R F ER V T R D L K V T R			M G GGMGAG K ST V L K E	
<i>S. italica-1</i>		-S T K K L R N V F M E A T R K Q R F AR V T R D L K V T R			M G GGMGAG K ST V L M E	
<i>Z. mays-1</i>		-S K R K L R N M V L E A T R K Q R F ER V T R D L K V T R			M G GGMGAG K ST V L K E	
Algae						
<i>K. flaccidum</i>		-K R H S L K R A V L S A T R T Q R Y K Q L L R S L G P Q R			M A GGMGAG K ST V R Q E	
<i>E. fimbriata</i>		--K-S L K G A V L R A T R T H R Y E R L V T A L G S Q R			M G GGMGAG K ST A A R R	
<i>Mougeotia sp.</i>		-K K M T F K A A V R K A T S I Q R V K K V I E H L G P Q R			I G GGMGAG K ST V - K E	
<i>Spyrogyra sp.</i>		-R L -S F K K A V L N A T R N Q R M E K I M T N F K T Q Q			L G GGMGAG K ST V A K Q	
<i>C. subellipsoidea</i>		n.d.			L G GG M A A G K ST V R E I	
<i>U. mutabilis</i>		n.d.			L G GG M A A G K SS V R N E	
<i>S. minuta</i>		n.d.			L G GGMGAG K ST A V K E	

Supplemental Figure S2. Features of NADKc primary sequence and its homologues in other plant and algae species. (A) putative CaM binding site (Arabidopsis NADKc amino acids 167-200). Red residues are those constituting the 1-5-8-14 motif. This domain is not conserved in *C. subellipsoidea*, *U. mutabilis* and *S. minuta*. *A. thaliana*: *Arabidopsis thaliana*, *S. phallax*: *Sphagnum phallax*, *P. patens*: *Physcomitrella patens*, *M. polymorpha*: *Marchantia polymorpha*, *S. mollendorffii*: *Selaginella mollendorffii*, *S. lycopersicum*: *Solanum lycopersicum*, *G. max*: *Glycine max*, *M. truncatula*: *Medicago truncatula*, *P. trichocarpa*: *Populus trichocarpa*, *M. acuminata*: *Musa acuminata*, *O. sativa*: *Oryza sativa*, *B. distachyon*: *Brachypodium distachyon*, *S. italica*: *Setaria italica*, *Z. mays*: *Zea mays*, *C. subellipsoidea*: *Coccomyxa subellipsoidea*, *U. mutabilis*: *Ulva mutabilis*, *S. minuta*: *Spirotaenia minuta*, *K. flaccidum*: *Klebsormidium flaccidum*, *E. fimbriata*: *Entransia fimbriata*. (B) Walker A motif (in red, residues characterizing the motif; *A. thaliana* NADKc amino acids 236-250). For gene references, see the legend of Fig. S6.

Figure S3

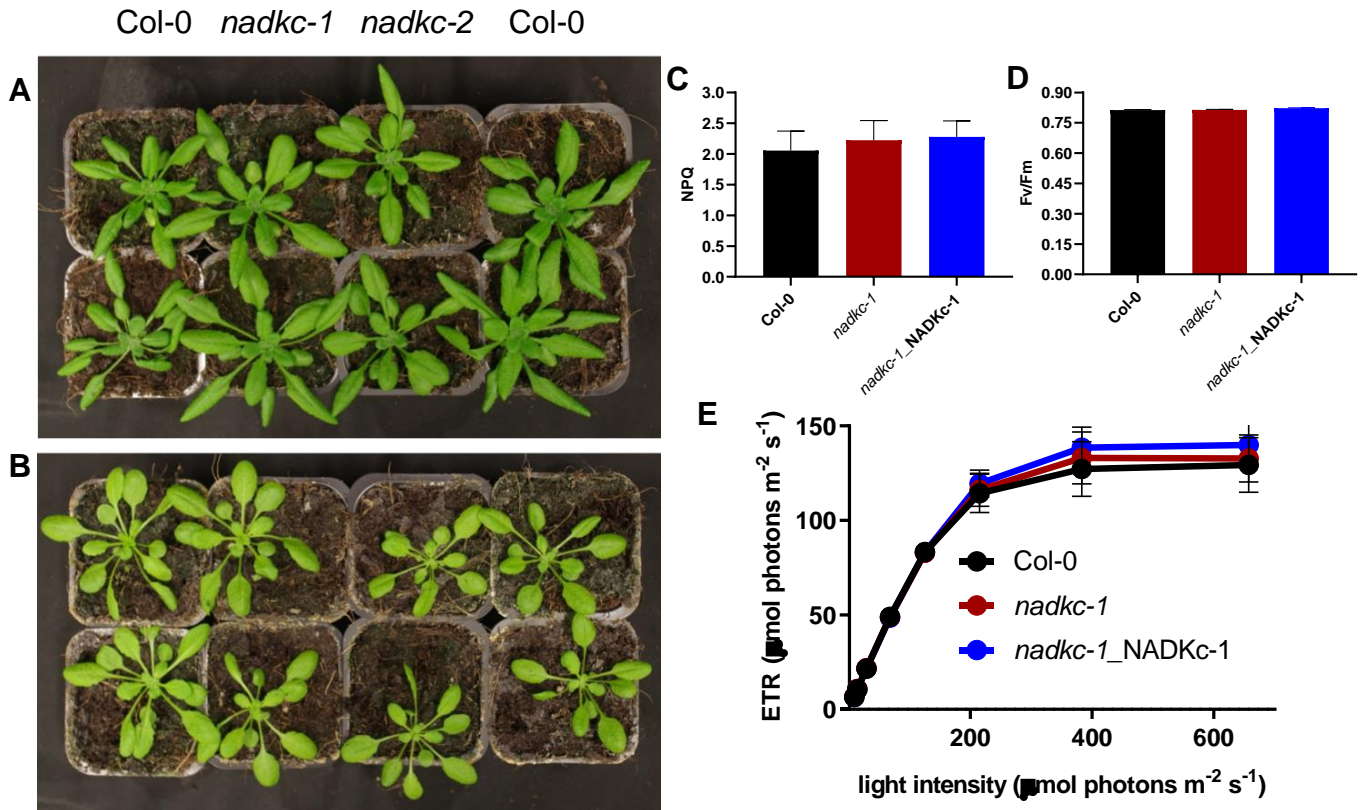


Supplemental Figure S3. Purification of recombinant NADKc produced in *E. coli*. 6HIS-Δ38NADKc was purified as indicated in Material and Methods. Lane 1: Rosetta2 soluble extract transformed with empty pET28a (40 μg); lane 2: Rosetta2 soluble extract transformed with pET28a6HIS-Δ38NADKc (40 μg); lane 3: Ni-NTA pool (10 μg); lane 4: urea-denatured 6HIS-Δ38NADKc purified on Ni-NTA (10 μg); lane 5: refolded 6HIS-Δ38NADKc (2 μg).

Figure S4

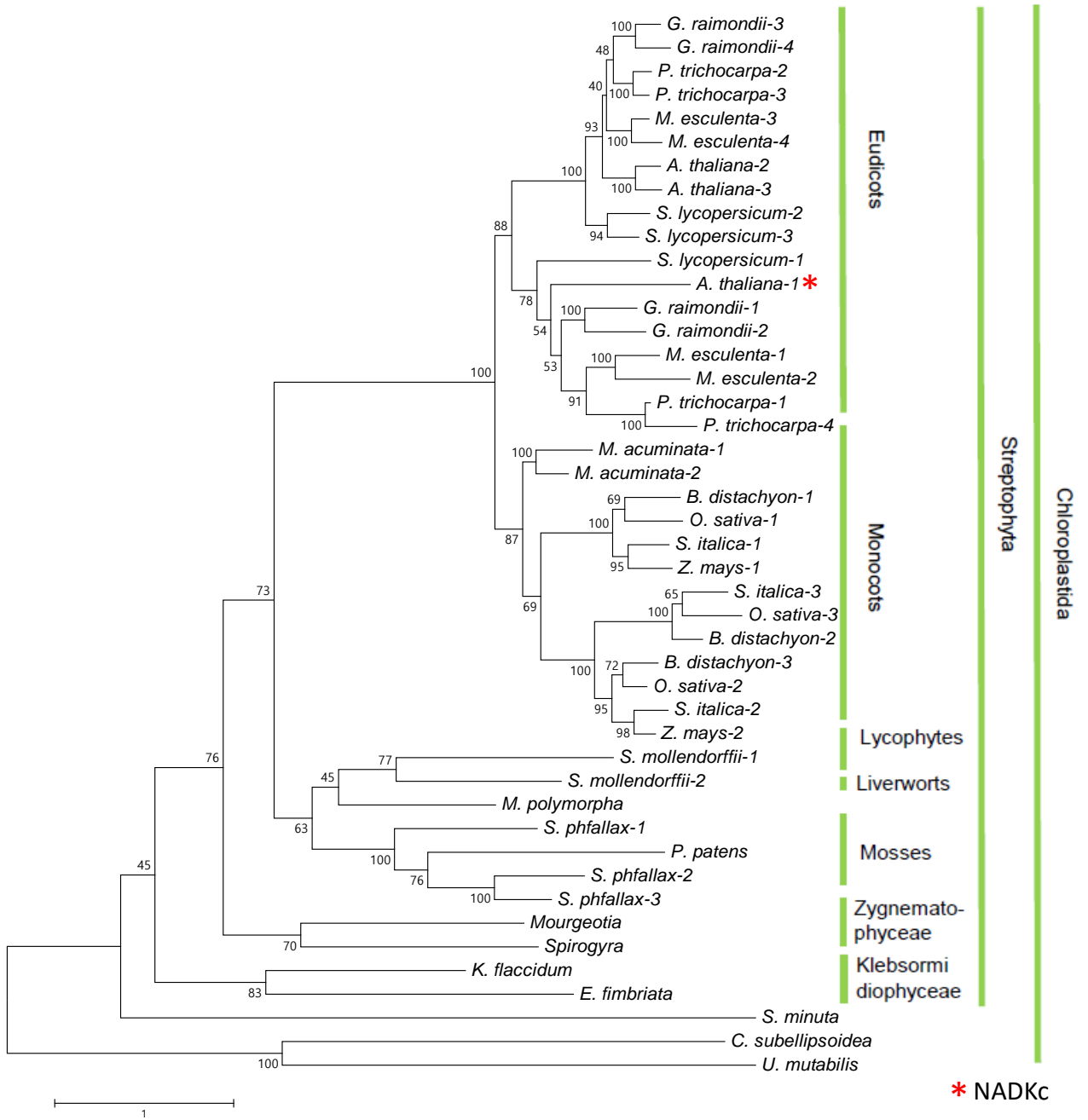
Supplemental Figure S4. A. NADKc_{Nter}-YFP associates with mitochondria in *N. benthamiana* leaves. Representative pictures of transiently transformed *N. benthamiana* leaf cells. Left: YFP (green), Center: RFP (red), and Right: merged fluorescence. The top row shows a representative image of *N. benthamiana* cells co-transformed with the NADKc_{Nter}-YFP construct and a mitochondrial marker, pSu9-RFP. The second row shows a close-up of mitochondria from the lower right region of the images in the top row (white boxes). White arrows indicate regions in which the YFP signal appears peripheral with respect to the RFP signal. The third row shows a representative image of *N. benthamiana* cells transformed with the YFP-NADKc construct alone. The central image shows the background signal in the RFP channel. White bars represent 2 μm in the first and second row, and 10 μm in the third row. **B.** Full length NADKc-YFP stably expressed in *Arabidopsis* forms aggregates in the cytosol. White bars represent 5 μm.

Figure S5



Supplemental Figure S5. Phenotype of *nadkc* mutants. (A) 21-day-old plants grown under long day photoperiod (16 h light/8 h dark); (B) 28-day-old plants grown under short day photoperiod (8 h light/16 h dark). (C-E) Photosynthetic parameters in Col-0 and *nadkc* plants: (C) NPQ, (D) Fv/Fm and (E) electron transport rate.

Figure S6



Supplementary Fig. S6. Phylogeny of NADKc. Maximum likelihood phylogenetic tree of NADKc-like proteins in the following plant and algal species: *Arabidopsis thaliana* (*A. thaliana*), *Populus trichocarpa* (*P. trichocarpa*), *Manihot esculenta* (*M. esculenta*), *Gossypium raimondii* (*G. raimondii*), *Solanum lycopersicum* (*S. lycopersicum*), *Setaria italica* (*S. italica*), *Zea mays* (*Z. mays*), *Oryza sativa* (*O. sativa*), *Brachypodium distachyon* (*B. distachyon*), *Musa acuminata* (*M. acuminata*), *Marchantia polymorpha* (*M. polymorpha*), *Physcomitrella patens* (*P. patens*), *Sphagnum phallax* (*S. phallax*), *Selaginella mollendorffii* (*S. mollendorffii*), *Klebsormidium flaccidum* (*K. flaccidum*), *Coccomyxa subellipsoidea* (*C. subellipsoidea*), *Ulva mutabilis* (*U. mutabilis*), *Spirotaenia minuta* (*S. minuta*), *Mougeotia* sp., *Spirogyra* sp. and *Entransia fimbriata* (*E. fimbriata*). Accession numbers: *A. thaliana*-1 (NADKc): At1g04280, *A. thaliana*-2: At1g06750, *A. thaliana*-3: At2g30630, *P. trichocarpa*-1: Potri.008G162000, *P. trichocarpa*-2: Potri.002G043000, *P. trichocarpa*-3: Potri.005G220000, *P. trichocarpa*-4: Potri.008G162400, *M. esculenta*-1: Manes.15G036900, *M. esculenta*-2: Manes.03G168900, *M. esculenta*-3: Manes.01G200600, *M. esculenta*-4: Manes.05G086200, *G. raimondii*-1: Gorai.011G171100, *G. raimondii*-2: Gorai.006G246600, *G. raimondii*-3: Gorai.004G074100, *G. raimondii*-4: Gorai.013G104300, *S. lycopersicum*-1: Solyc06g053810, *S. lycopersicum*-2: Solyc06g031670, *S. lycopersicum*-3: Solyc08g059750, *S. italica*-1: Seita.9G163700, *S. italica*-2: Seita.3G185100, *S. italica*-3: Seita.5G337000, *Z. mays*-1: GRMZM2G070252, *Z. mays*-2: GRMZM2G368410, *O. sativa*-1: Os03g43010, *O. sativa*-2: Os05g43300, *O. sativa*-3: Os01g56764, *B. distachyon*-1: Bradi1g14307, *B. distachyon*-2: Bradi2g51490, *B. distachyon*-3: Bradi2g20400, *M. acuminata*-1: SMUA_Achr5T03210, *M. acuminata*-2: GSMUA_Achr7T01560, *M. polymorpha*: Mapoly0142s0012, *P. patens*: Pp3c2_3490V3, *S. phallax*-1: Sphallax0059s0037, *S. phallax*-2: Sphallax0011s0002, *S. phallax*-3: Sphallax0120s0019, *S. mollendorffii*-1: scaffold 73427, *S. mollendorffii*-2: scaffold 231175, *K. flaccidum*: kfl00274_0130, *C. subellipsoidea*: XP_005648203, *U. mutabilis*: UM028_0076.1, *S. minuta*: NNHQ_2000691, *Mougeotia*: ZRMT_2002068, *Spirogyra*: HAOX_2025158, *E. fimbriata*: BFIK_2025349. The tree is drawn to scale, with branch lengths measured in the number of substitutions per site (scale bar in the bottom-left corner). The numbers at the interior nodes are bootstrap percentages.

Table S2: Primers used in this study

In red: sequences for recombination reactions by BP clonase into pDONR221.

Uppercase: restriction enzyme sites.

Primers for cloning the NADKc protein sequence for enzymatic, localization and complementation studies:

construct	Forward primer	Reverse primer
pet28(b)-6-HIS-NADKc	gacttttcaaaccacCATATGgtgaaac ccttaggagaag	caaattcaggaagaagaCTCGAGcaaagg tctagttc
pet28(b)-6-HIS-D38NADKc	gctgtagcagctCATATGgccggagaat tactc	caaattcaggaagaagaCTCGAGcaaagg tctagttc
35S::NADKc _{Nter} -YFP (in pB7YWG2,0)	GGGGACAAGTTTGTACAAAAAGCAGGC TTgatggtgaaacccttaggagaag	GGGGACCACTTTGTACAAGAAAGCTGGGT ggacatctttataccccatg
35S::NADKc-YFP (in pB7YWG2,0)	GGGGACAAGTTTGTACAAAAAGCAGGC TTgatggtgaaacccttaggagaag	GGGGACCACTTTGTACAAGAAAGCTGGGT atTTTTTggttgggccttttcgattctcc
35S::YFP-NADKc (in pB7WGY2,0) and 35S::NADKc (in pB2GW7,0)	GGGGACAAGTTTGTACAAAAAGCAGGC TTgatggtgaaacccttaggagaag	GGGGACCACTTTGTACAAGAAAGCTGGGT tcaatTTTTTggttgggccttttcgattc tcc

Primers for genotyping:

line	Forward primer	Reverse primer	LB primer
SALK_130871	tgtaaagcaaatatgtg ggcc	acaaatgatcgaaatgg caag	LBb1.3 atTTTgccgattttcgg aac
GABI_311H11	taaggaagaaggacggg acttc	tcaagatcgaccaaacg attag	LBgabi-kat atattgaccatcatact cattgc

Primers for gene expression studies (qPCR):

	Forward primer	Reverse primer
At1g04280	aacgggtcagcagtcctcaa c	gggcctcgatggaactaac a